

Supplementary Information

Reactions of polyaromatic molecules in crystals under electron beam of the transmission electron microscope

Kayleigh L. Y. Fung, Benjamin L. Weare, Michael W. Fay, Stephen P. Argent, Andrei N. Khlobystov.

Contents

1	Transmission Electron Microscopy Details	3
2	Selected area electron diffraction time series	4
2.1	SAED of perchlorocoronene crystals	4
2.2	SAED of hexadecachloro-copper(II) phthalocyanine crystals	5
2.3	SAED of coronene crystals	6
2.4	SAED of copper(II) phthalocyanine crystals	7
3	Spot intensities of diffraction patterns over time	8
3.1	Intensities over time of SAED spots for perchlorocoronene and hexadecachloro-copper(II) phthalocyanine crystals	8
3.2	Intensities over time of SAED spots for coronene and copper(II) phthalocyanine crystals	9
3.3	Intensities over time of SAED spots for hexaazatrinaphthylene derivatives	10
4	EDX spectra during irradiation	11
4.1	EDX spectra of hexachloro-hexaazatrinaphthylene crystals	11
4.2	EDX spectra of hexafluoro-hexaazatrinaphthylene crystals	13
4.3	EDX spectra of hexaazatrinaphthylene crystals	15
5	Information on crystal planes	17

5.1	Perchlorocoronene crystal planes	17
5.2	Coronene crystal planes	18
5.3	Hexaazatrinaphthylene crystal planes	19
5.4	Hexachloro-hexaazatrinaphthylene crystal planes	20
5.5	Hexafluoro-hexaazatrinaphthylene crystal planes	21
6	Synthesis and characterisation	22
6.1	Perchlorocoronene	22
6.2	H-HATN	24
6.3	Cl ₆ -HATN	30
6.4	F ₆ -HATN	35
7	SCXRD refinement and data	36
7.1	Refinement details for 5,6,11,12,17,18- hexaazatrinaphthylene	36
7.2	Refinement details for 2,3,8,9,14,15- hexafluoro- 5,6,11,12,17,18- hex- aazatrinaphthylene	42
7.3	SCXRD data for 5,6,11,12,17,18- hexaazatrinaphthylene and 2,3,8,9,14,15- hexafluoro- 5,6,11,12,17,18- hexaazatrinaphthylene.	42

1 Transmission Electron Microscopy Details

Transmission electron microscopy (TEM) was performed using a JEOL 2100F TEM (field emission electron gun, information limit 0.19 nm) and a JEOL 2100 Plus TEM (LaB6 instrument, information limit 0.40 nm) with an accelerating voltage of 80 kV at the Nanoscale and Microscale Research Centre at the University of Nottingham. TEM samples were prepared by gently grinding the crystals in an agate mortar and pestle before pressing onto a copper grid mounted with “lacey” carbon films (Agar Scientific UK). The specific diffraction conditions used the second smallest condenser aperture (40 μm), alpha 3, spot size 5, with the beam completely spread. Beam intensity was measured at these conditions in imaging mode at 8000x magnification before switching to diffraction mode at a camera length of 250mm. The micrographs were acquired with a 0.5 s capture time. All micrographs were processed using Gatan Digital Micrograph and ImageJ Fiji software.¹⁻³ Energy dispersive X-ray spectroscopy (EDXS) was acquired using an Oxford Instruments X-Max 80 and an XMax 100 TLE, and analysed using the AZtec X-ray microanalysis system. $K\alpha$ values were used for carbon (0.277 keV), nitrogen (0.392 keV), fluorine (0.677 keV), and chlorine (2.622 keV). Diffraction data was analysed using CrystBox.⁴⁻⁶

2 Selected area electron diffraction time series

2.1 SAED of perchlorocoronene crystals

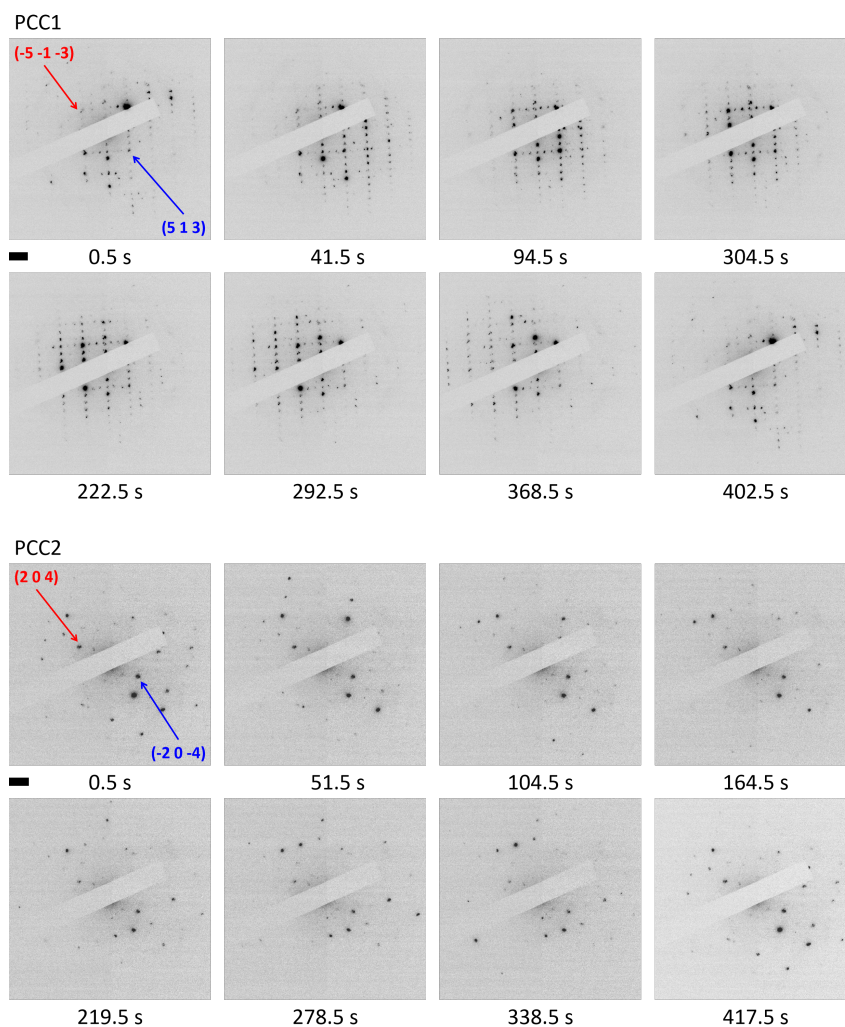


Figure 1. Diffraction pattern series of nanocrystals of perchlorocoronene. The time stamps are shown below each pattern. The scale bar is 2 nm^{-1} . PCC1: The tracked pair of diffraction spots have a d-spacing of 3.01 \AA . More information on the planes corresponding to the diffraction spots can be found in the SI. PCC1 was irradiated using an electron flux of $9.94 \times 10 \text{ e}^- \text{ nm}^{-2} \text{ s}^{-1}$ over a period of 402.5 s for a total electron fluence of $4.00 \times 10^4 \text{ e}^- \text{ nm}^{-2}$. PCC2: The tracked pair of diffraction spots have a d-spacing of 2.96 \AA . More information on the planes corresponding to the diffraction spots can be found in Fig. 11 in the SI. PCC2 was irradiated using an electron flux of $9.65 \times 10 \text{ e}^- \text{ nm}^{-2} \text{ s}^{-1}$ over a period of 417.5 s for a total electron fluence of $4.03 \times 10^4 \text{ e}^- \text{ nm}^{-2}$.

2.2 SAED of hexadecachloro-copper(II) phthalocyanine crystals

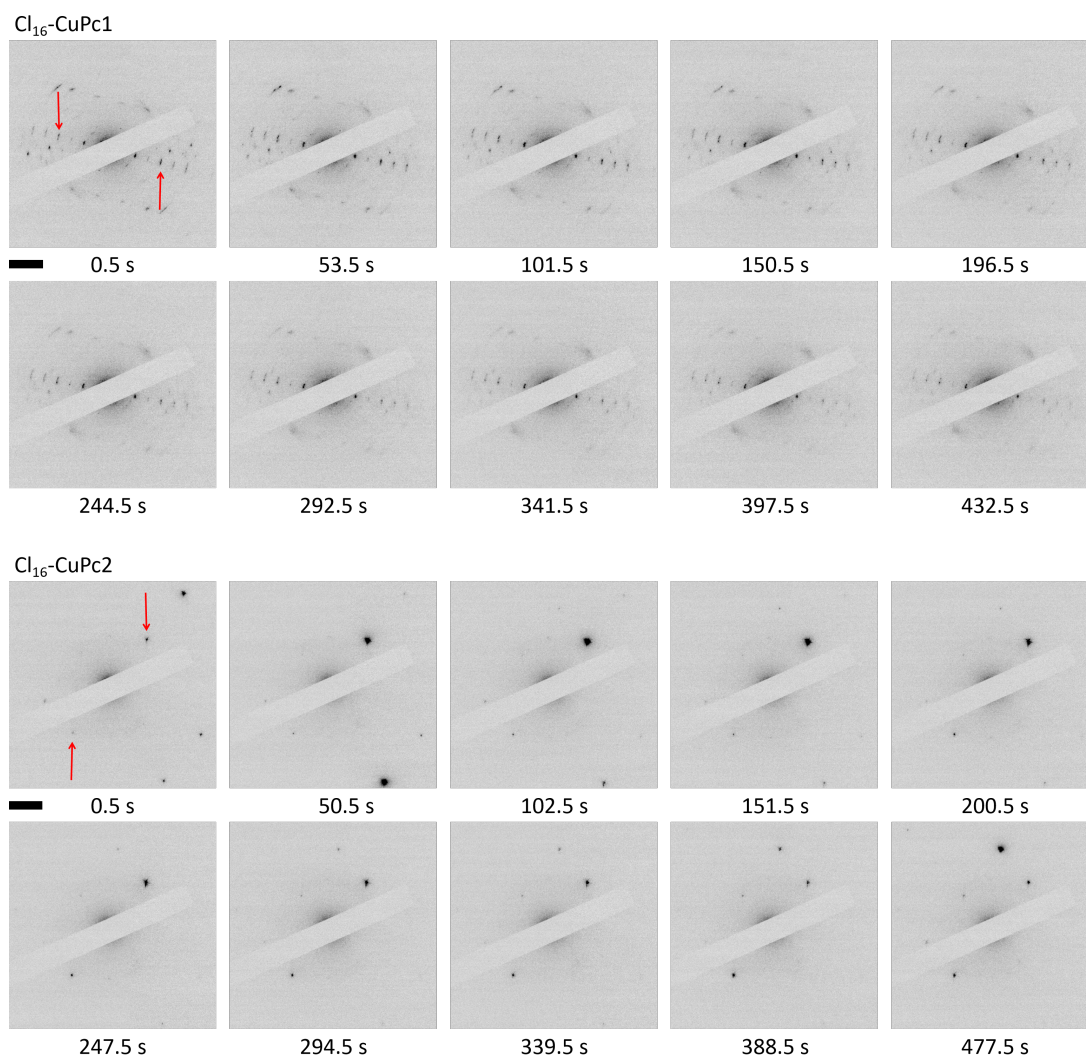


Figure 2. Diffraction pattern series of nanocrystals of hexadecachloro-copper(II) phthalocyanine. The time stamps are shown below each pattern. The scale bar is 2 nm^{-1} . Cl₁₆-CuPc: The tracked pair of diffraction spots have a d-spacing of 3.27 \AA . Cl₁₆-CuPc was irradiated using an electron flux of $9.25 \times 10 \text{ e}^- \text{ nm}^{-2} \text{ s}^{-1}$ over a period of 432.5 s for a total electron fluence of $4.00 \times 10^4 \text{ e}^- \text{ nm}^{-2}$. Cl₁₆-CuPc2: The tracked pair of diffraction spots have a d-spacing of 2.85 \AA . Cl₁₆-CuPc2 was irradiated using an electron flux of $8.38 \times 10 \text{ e}^- \text{ nm}^{-2} \text{ s}^{-1}$ over a period of 477.5 s for a total electron fluence of $4.00 \times 10^4 \text{ e}^- \text{ nm}^{-2}$.

2.3 SAED of coronene crystals

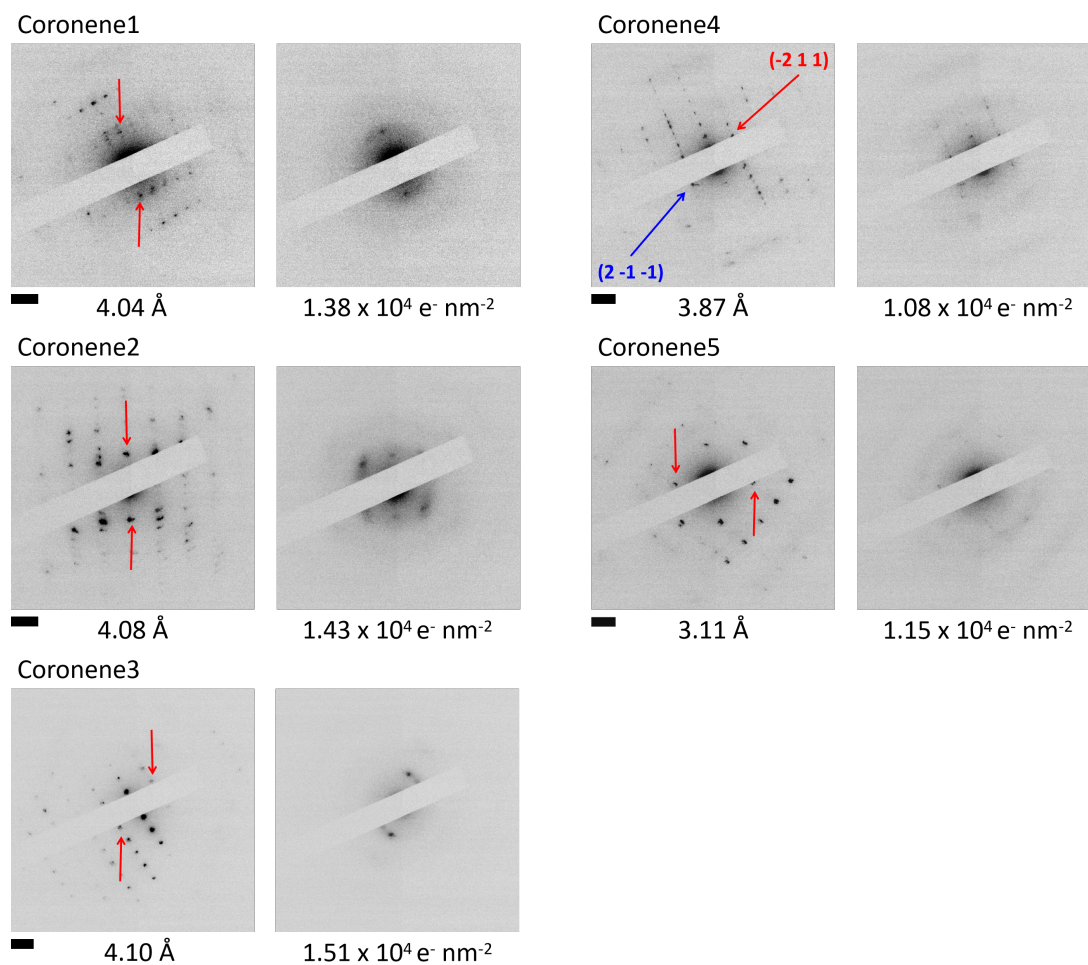


Figure 3. Diffraction pattern series of nanocrystals of coronene. The d-spacings of the tracked pairs of diffraction spots and the critical fluences are shown below the micrographs. More information on the planes corresponding to the diffraction spots of Coronene4 can be found in Fig. 12 in the SI. The scale bars are 2 nm^{-1} . The nanocrystals were irradiated using an average electron flux of $9.14 \times 10 \text{ e}^- \text{ nm}^{-2} \text{ s}^{-1}$ over an average period of 143.7 s for an average total electron fluence of $1.31 \times 10^4 \text{ e}^- \text{ nm}^{-2}$.

2.4 SAED of copper(II) phthalocyanine crystals

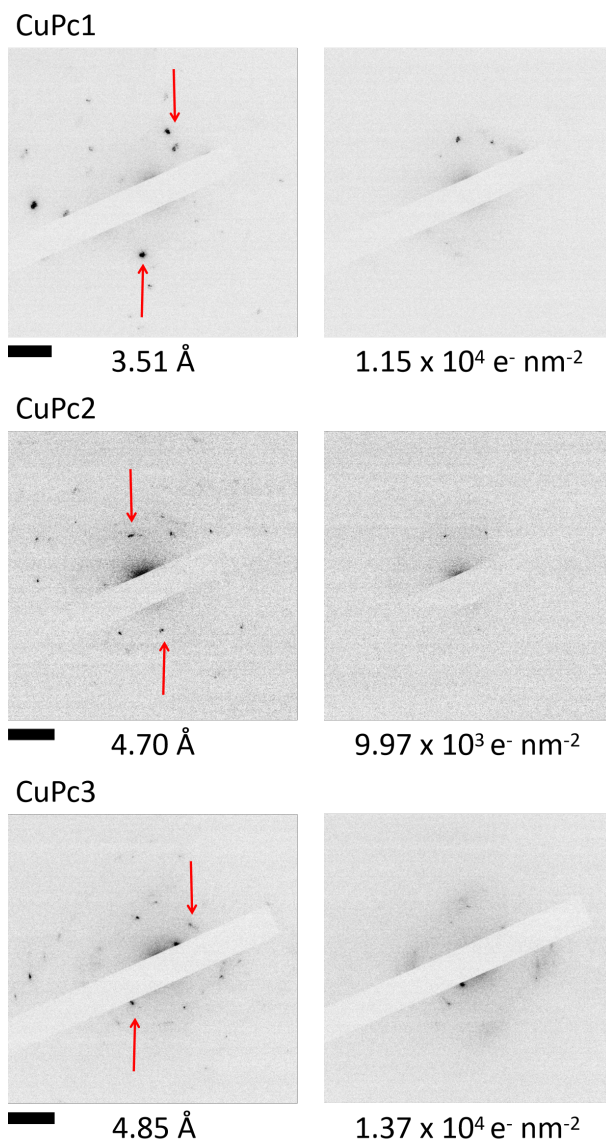


Figure 4. Diffraction pattern series of nanocrystals of copper(II) phthalocyanine (CuPc). The d-spacings of the tracked pairs of diffraction spots and the critical fluences are shown below the micrographs. The scale bars are 2 nm^{-1} . The nanocrystals were irradiated using an average electron flux of $9.29 \times 10 \text{ e}^- \text{ nm}^{-2} \text{ s}^{-1}$ over an average period of 125.8 s for an average total electron fluence of $1.17 \times 10^4 \text{ e}^- \text{ nm}^{-2}$.

3 Spot intensities of diffraction patterns over time

3.1 Intensities over time of SAED spots for perchlorocoronene and hexadecachloro-copper(II) phthalocyanine crystals

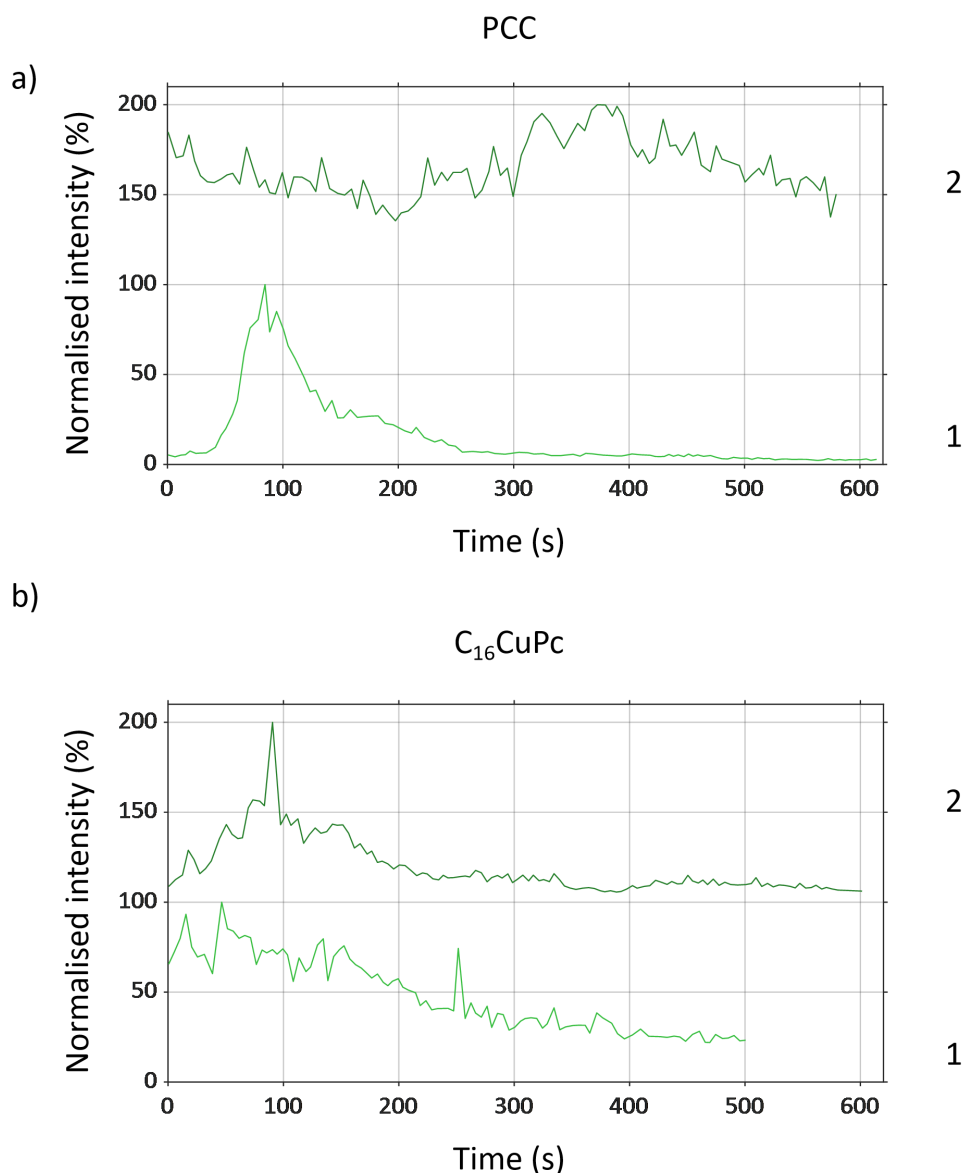


Figure 5. Normalised intensities over time of a) PCC1 (light green), PCC2 (dark green), b) C_{16} -CuPc1 (light green), and C_{16} -CuPc2 (dark green). PCC2 and C_{16} -CuPc2 have been offset by 100% for clarity, appearing between 100 and 200% on the plot. All crystals were irradiated with electron fluxes on the order of $10 \text{ e}^- \text{ nm}^{-2} \text{ s}^{-1}$. Note that for PCC1, the diffraction spot intensity appears to be negligible at the beginning of irradiation. The crystal rotating and/or translating during irradiation led to a huge increase in the intensity of the tracked pair of diffraction spots, leading to a seemingly low diffraction spot intensity at the beginning.

3.2 Intensities over time of SAED spots for coronene and copper(II) phthalocyanine crystals

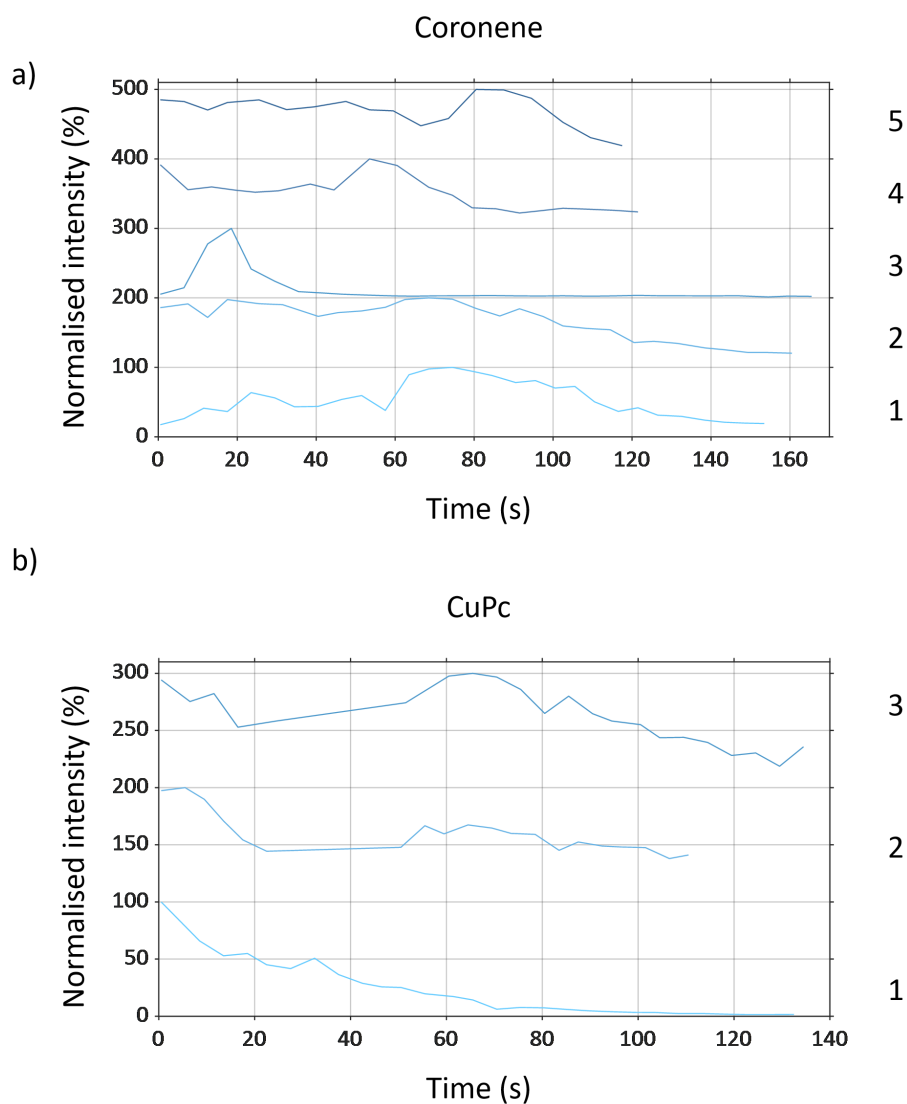


Figure 6. Normalised intensities over time of a) Coronene1-5 from bottom to top and b) CuPc1-3 from bottom to top. All plots have been offset from one another by 100% for clarity. All crystals were irradiated with electron fluxes on the order of $10 \text{ e}^- \text{ nm}^{-2} \text{ s}^{-1}$.

3.3 Intensities over time of SAED spots for hexaazatrinaphthylene derivatives

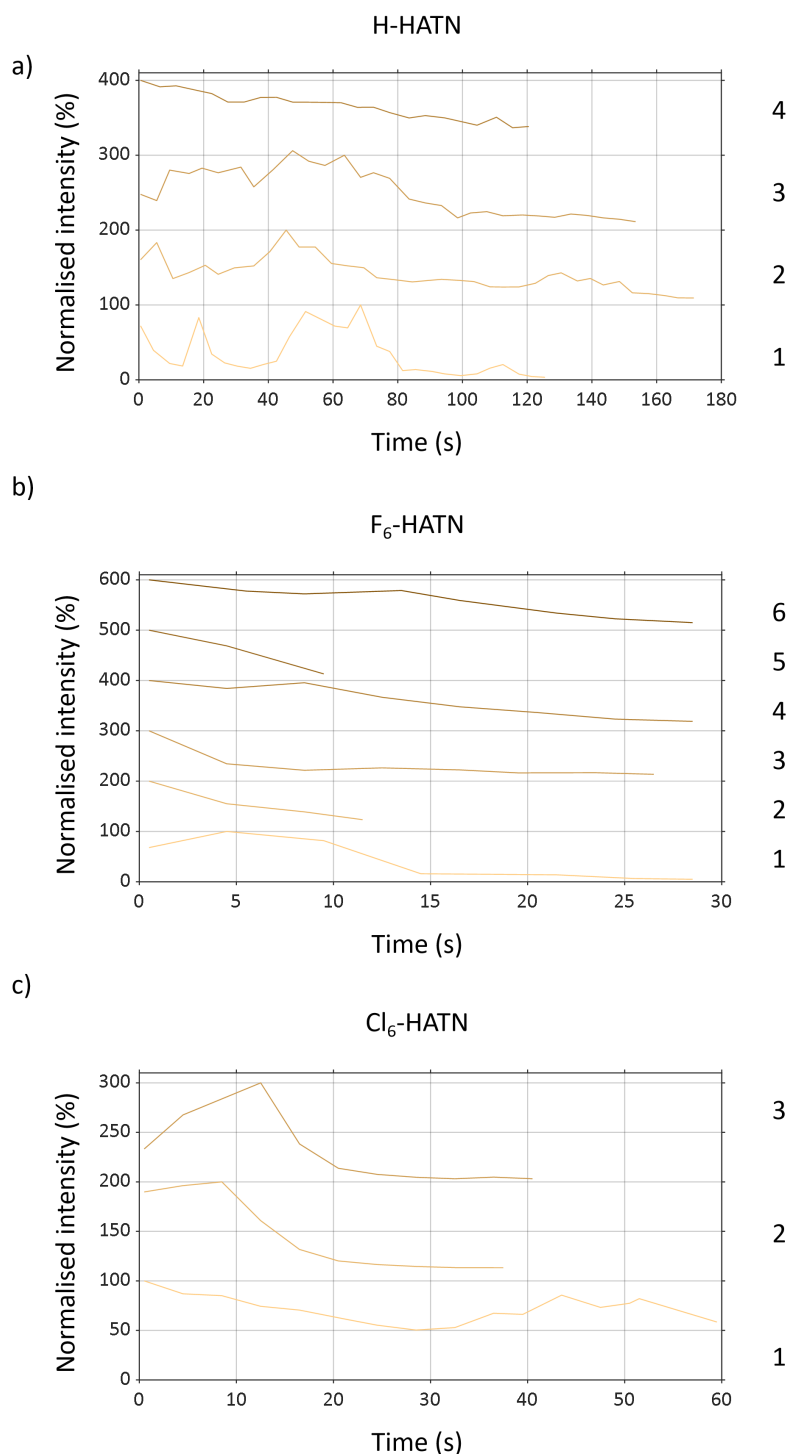


Figure 7. Normalised intensities over time of a) H-HATN1-4 from bottom to top, b) F₆-HATN1-6 from bottom to top, and c) Cl₆-HATN1-3 from bottom to top. All plots have been offset from one another by 100% for clarity. All crystals were irradiated with electron fluxes on the order of $10\text{-}10^2 \text{ e}^- \text{ nm}^{-2} \text{ s}^{-1}$.

4 EDX spectra during irradiation

4.1 EDX spectra of hexachloro-hexaazatrinaphthylene crystals

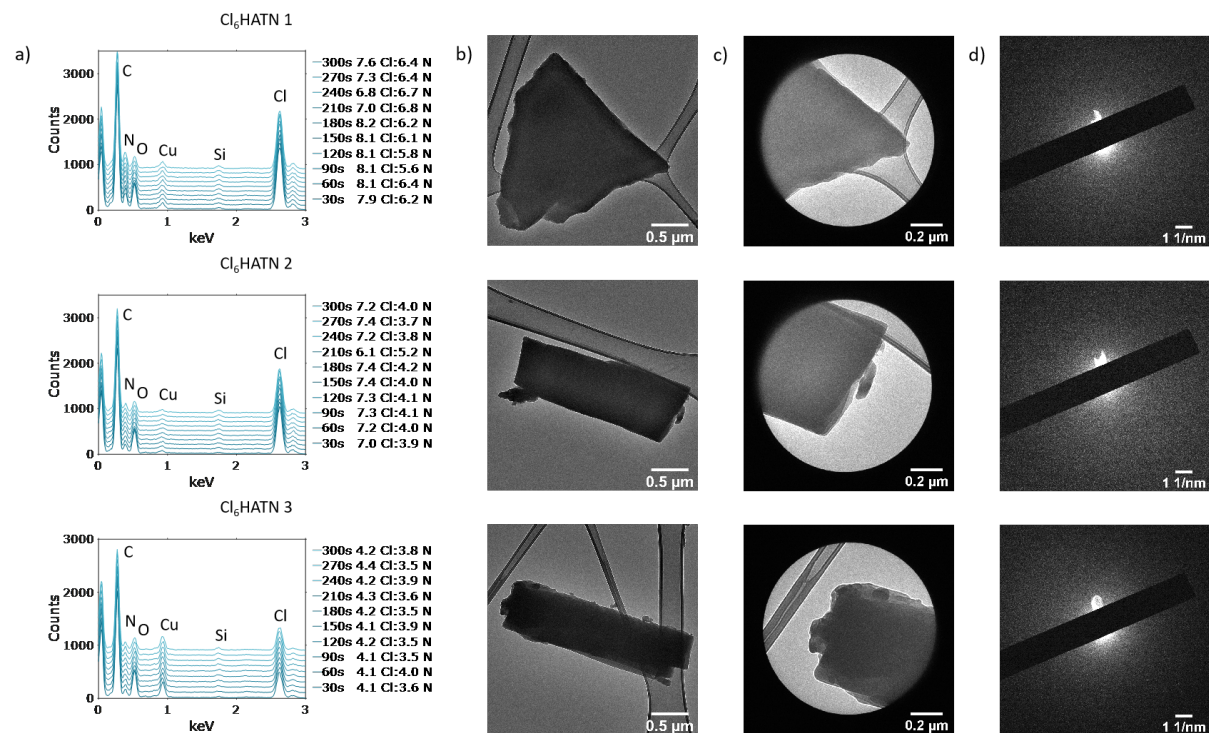


Figure 8. a) Energy dispersive X-ray (EDX) spectra acquired over 300 s of Cl₆-HATN 1-3 crystals. Spectra have been offset from each other for clarity. The electron flux was kept constant at $10^1 \text{ e}^- \text{ nm}^{-2} \text{ s}^{-1}$. There is no significant change in Cl:N ratios before and after irradiation. Cu signal is from the copper grid; Si signal is contamination from glassware used to store the sample. b) Micrographs of the irradiated Cl₆-HATN 1-3 crystals. c) Micrographs of selected areas of Cl₆-HATN crystals 1-3 for electron diffraction after irradiation. d) Selected area electron diffraction of Cl₆-HATN crystals 1-3 after irradiation showing that the samples are amorphous.

4.2 EDX spectra of hexafluoro-hexaazatrinaphthylene crystals

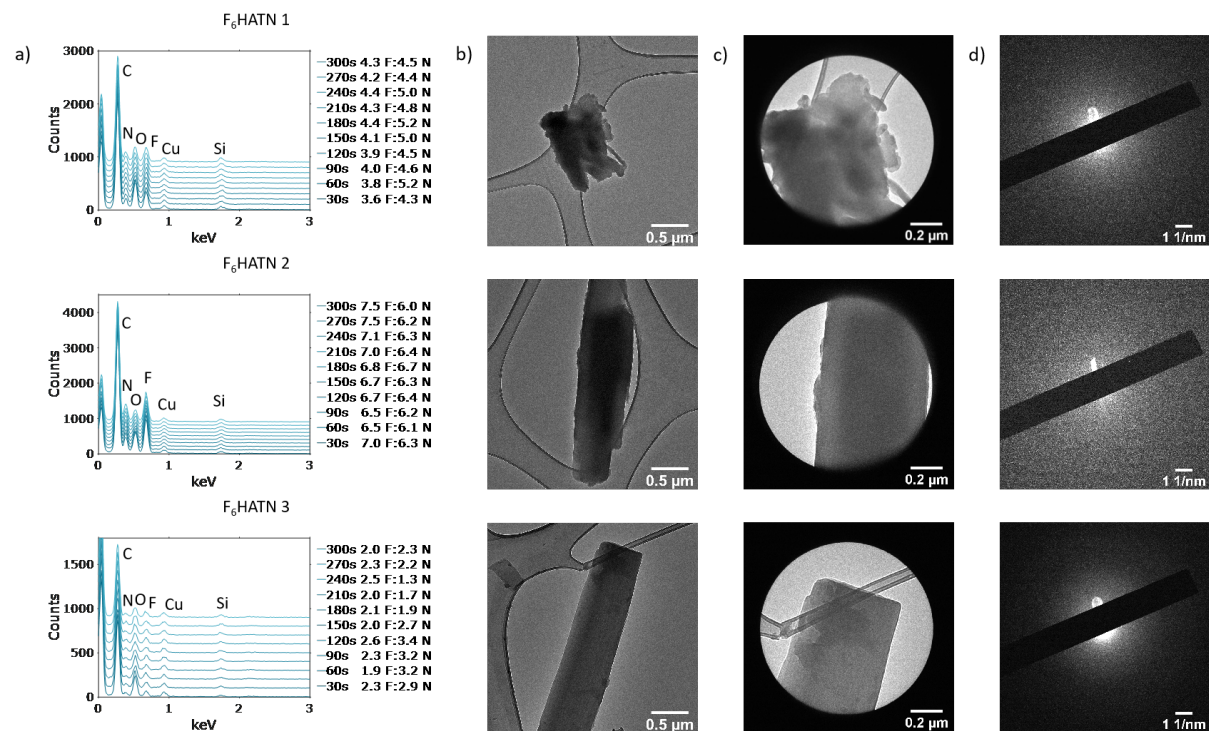


Figure 9. a) Energy dispersive X-ray (EDX) spectra acquired over 300 s of F₆-HATN 1-3 crystals. Spectra have been offset from each other for clarity. The electron flux was kept constant at $10^1 \text{ e}^- \text{ nm}^{-2} \text{ s}^{-1}$. There is no significant change in F:N ratios before and after irradiation. Cu signal is from the copper grid; Si signal is contamination from glassware used to store the sample. b) Micrographs of the irradiated F₆-HATN 1-3 crystals. c) Micrographs of selected areas of F₆-HATN crystals 1-3 for electron diffraction after irradiation. d) Selected area electron diffraction of F₆-HATN crystals 1-3 after irradiation showing that the samples are amorphous.

4.3 EDX spectra of hexaazatrinaphthylene crystals

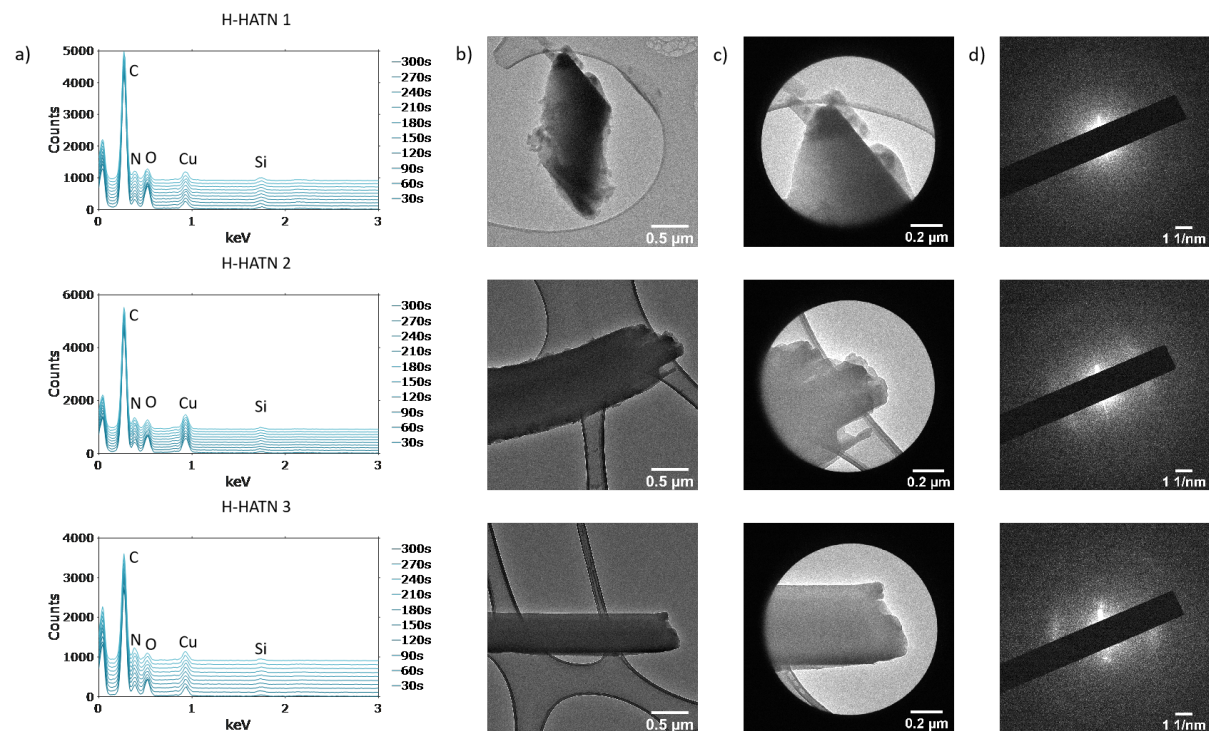


Figure 10. a) Energy dispersive X-ray (EDX) spectra acquired over 300 s of H-HATN 1-3 crystals. Spectra have been offset from each other for clarity. The electron flux was kept constant at $10^1 \text{ e}^- \text{ nm}^{-2} \text{ s}^{-1}$. Cu signal is from the copper grid; Si signal is contamination from glassware used to store the sample. b) Micrographs of the irradiated H-HATN 1-3 crystals. c) Micrographs of selected areas of H-HATN crystals 1-3 for electron diffraction after irradiation. d) Selected area electron diffraction of H-HATN crystals 1-3 after irradiation showing that the samples are amorphous.

5 Information on crystal planes

5.1 Perchlorocoronene crystal planes

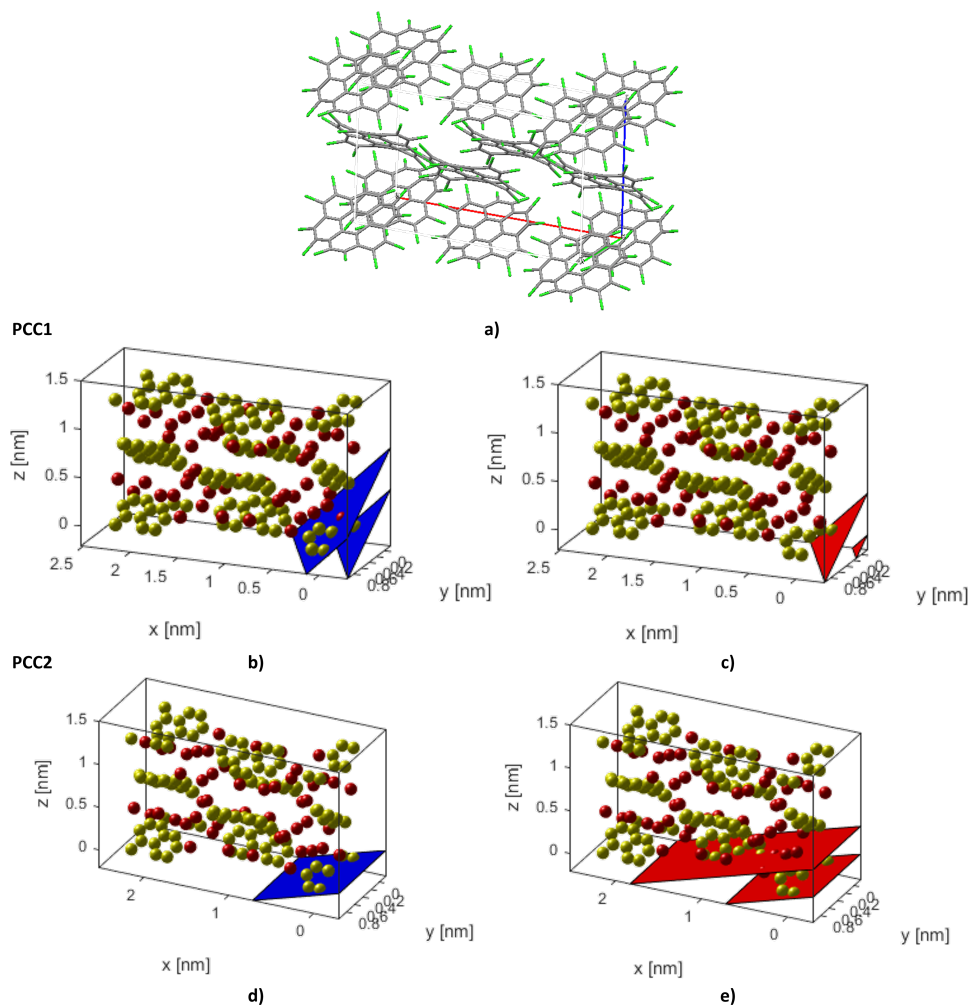


Figure 11. a) The unit cell of perchlorocoronene (PCC).⁷ b) and c) The unit cell of PCC with the same orientation as a) where blue corresponds to the (5 1 3) plane and red corresponds to the (-5 -1 -3) plane. These planes correspond to the tracked pair of diffraction spots for the PCC1 crystal. d) and e) The unit cell of PCC with the same orientation as a) where blue corresponds to the (-2 0 -4) plane and red corresponds to the (2 0 4) plane. These planes correspond to the tracked pair of diffraction spots for the PCC2 crystal. Images were generated by the cellViewer program in CrysTBox.⁴⁻⁶ The assignments for PCC1 and PCC2 were carried out using the diffractGUI program in CrysTBox, giving a d-spacing standard deviation of 0.0013 and 0.0023, and structural factor deviations (R-square values) of 0.9816 and 1.0000 respectively.

5.2 Coronene crystal planes

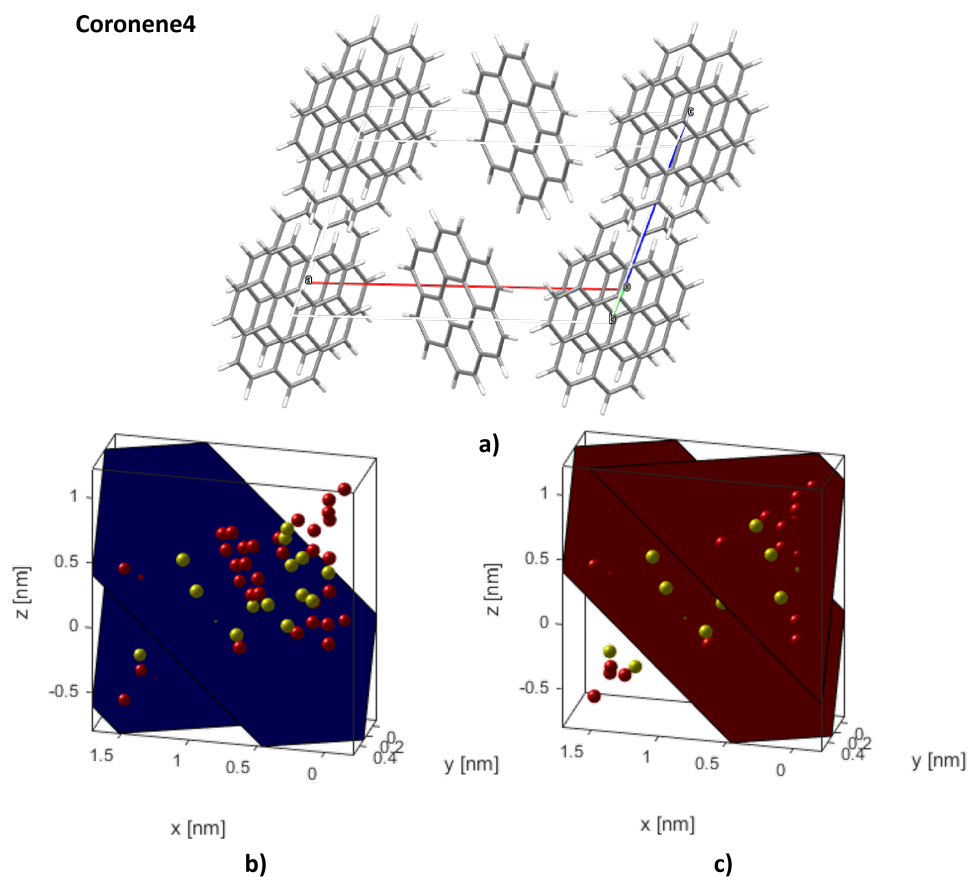


Figure 12. a) The unit cell of coronene.⁸ b) and c) The unit cell of coronene with the same orientation as a) where blue corresponds to the (2 -1 -1) plane and red corresponds to the (-2 1 1) plane. These planes correspond to the tracked pair of diffraction spots for the coronene4 crystal (Fig. 3). Images were generated by the cellViewer program in CrysTBox.⁴⁻⁶ The assignments for coronene4 were carried out using the diffractGUI program in CrysTBox, giving a d-spacing standard deviation of 0.0016 and a structural factor deviation (R-square value) of 0.9814.

5.3 Hexaazatrinaphthylene crystal planes

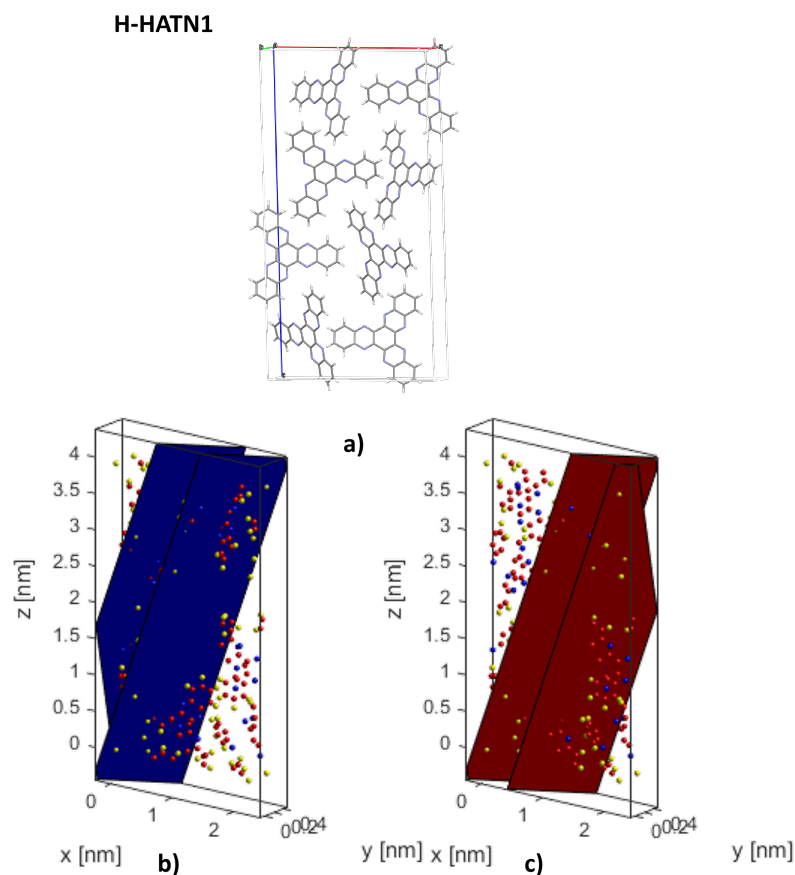


Figure 13. a) The unit cell of 5,6,11,12,17,18- hexaazatrinaphthylene (H-HAT). b) and c) The unit cell of H-HAT with the same orientation as a) where blue corresponds to the $(-3 \ 1 \ 2)$ plane and red corresponds to the $(3 \ -1 \ -2)$ plane. These planes correspond to the tracked pair of diffraction spots for the H-HAT1 crystal. Images were generated by the cellViewer program in CrystBox.⁴⁻⁶ The assignments for H-HAT1 were carried out using the diffractGUI program in CrystBox, giving a d-spacing standard deviation of 0.0042 and a structural factor deviation (R-square value) of 0.9119.

5.4 Hexachloro-hexaazatrinaphthylene crystal planes

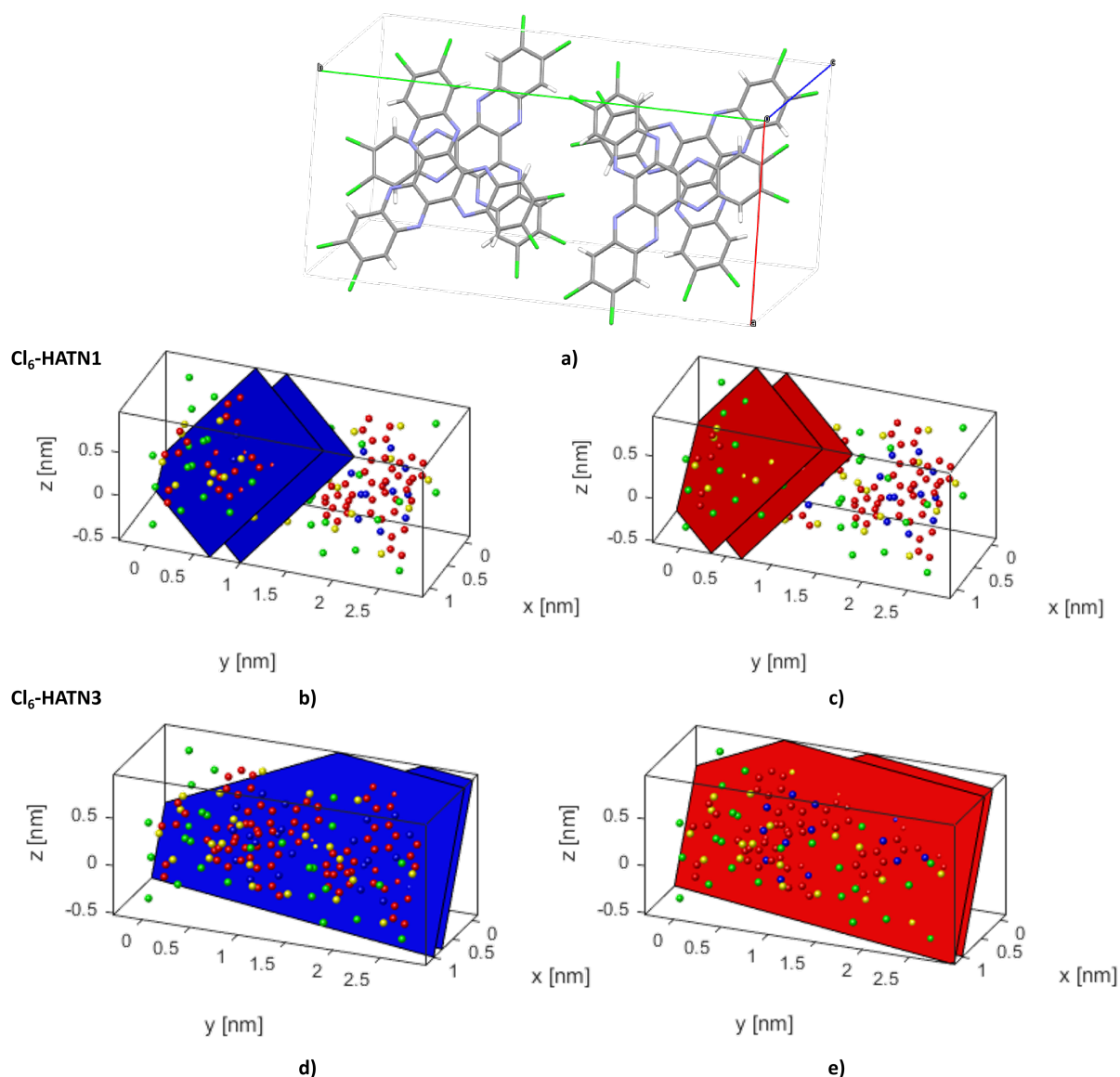


Figure 14. a) The unit cell of 2,3,8,9,14,15- hexachloro- 5,6,11,12,17,18- hexaazatrinaphthylene.⁹ b) and c) The unit cell of Cl₆-HAT with the same orientation as a) where blue corresponds to the $(-2\ 8\ -2)$ plane and red corresponds to the $(2\ -8\ 2)$ plane. d) and e) The unit cell of Cl₆-HAT with the same orientation as a) where blue corresponds to the $(-4\ 3\ -2)$ plane and red corresponds to the $(4\ -3\ 2)$ plane. Images were generated by the cellViewer program in CrystBox.⁴⁻⁶ The assignments for Cl₆-HAT1 and Cl₆-HAT3 were carried out using the diffractGUI program in CrystBox, giving d-spacing standard deviations of 0.0026 and 0.0009 and structural factor deviations (R-square values) of 0.8722 and 0.9680 respectively.

5.5 Hexafluoro-hexaazatrinaphthylene crystal planes

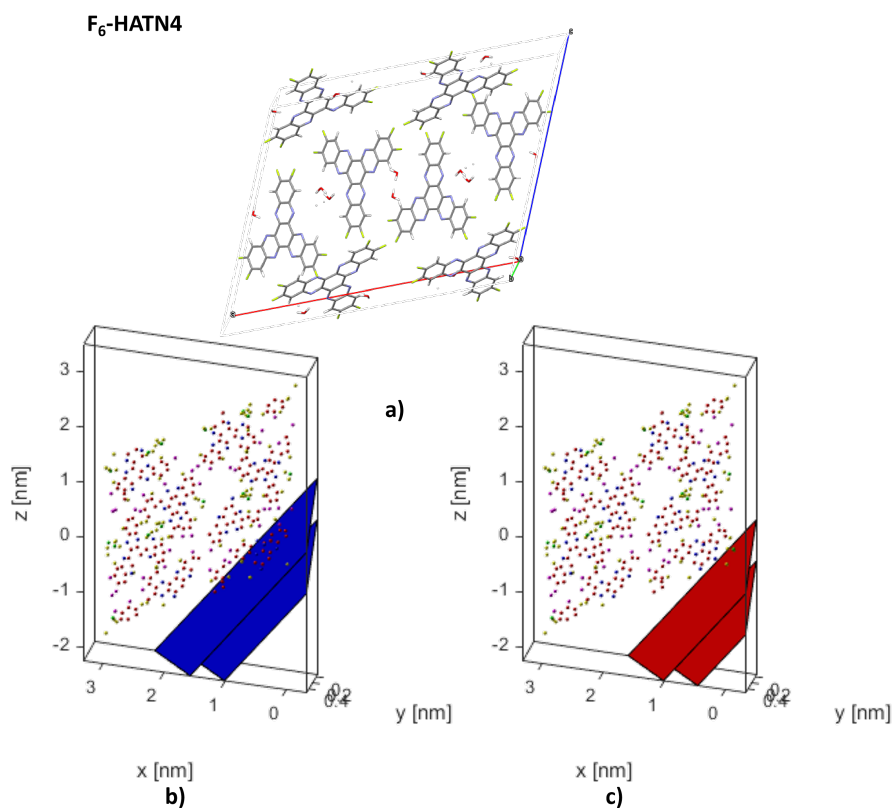


Figure 15. a) The unit cell of 2,3,8,9,14,15- hexafluoro- 5,6,11,12,17,18- hexaazatrinaphthylene (F₆-HAT). b) and c) The unit cell of F₆-HAT with the same orientation as a) where blue corresponds to the (3 1 4) plane and red corresponds to the (-3 -1 -4) plane. These planes correspond to the tracked pair of diffraction spots for the F₆-HAT4 crystal. Images were generated by the cellViewer program in CrystBox.⁴⁻⁶ The assignments for F₆-HAT4 were carried out using the diffractGUI program in CrystBox, giving a d-spacing standard deviation of 0.0014 and a structural factor deviation (R-square value) of 0.9253.

6 Synthesis and characterisation

6.1 Perchlorocoronene

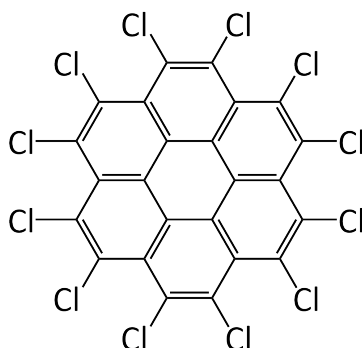


Figure 16. Perchlorocoronene.

Synthesis of perchlorocoronene was taken from literature^{10,11} and is described here. Aluminium chloride (7.5 mg) was dissolved in sulfuryl chloride (3 ml) and heated to reflux (70 °C). A mixture of coronene (30 mg) and sulfur monochloride (8.89 μ l) in sulfuryl chloride (5 ml) was added dropwise to the reflux over 3 min. The reaction turned inky blue upon addition of the coronene mixture. The solvent volume was reduced to approximately 1 ml by distillation and left to reflux (70 °C) for 28 hours. Additional sulfuryl chloride was added throughout the reflux to maintain the solvent volume. The resulting dark yellow suspension was distilled to dryness and neutralised with deionised water and sodium bicarbonate, heated to 95 °C for 1 hr, and then acidified with hydrochloric acid (37%, pH 1). The mixture was filtered through a PTFE membrane (0.2 μ m pore size), washed with deionised water, and dried under vacuum. No purification was required. The product, perchlorocoronene was a dark yellow powder (72 mg, quant.). ¹³C NMR δ (500 MHz, CDCl₃); 133.2 (Aryl C-Cl), 126.8 (Aryl C), 121.4 (Aryl C). Positive-ion MALDI-ToF MS m/z; 713 (C₂₄Cl₁₂), 642 (C₂₄Cl₁₀), 571 (C₂₄Cl₈), 500 (C₂₄Cl₆).

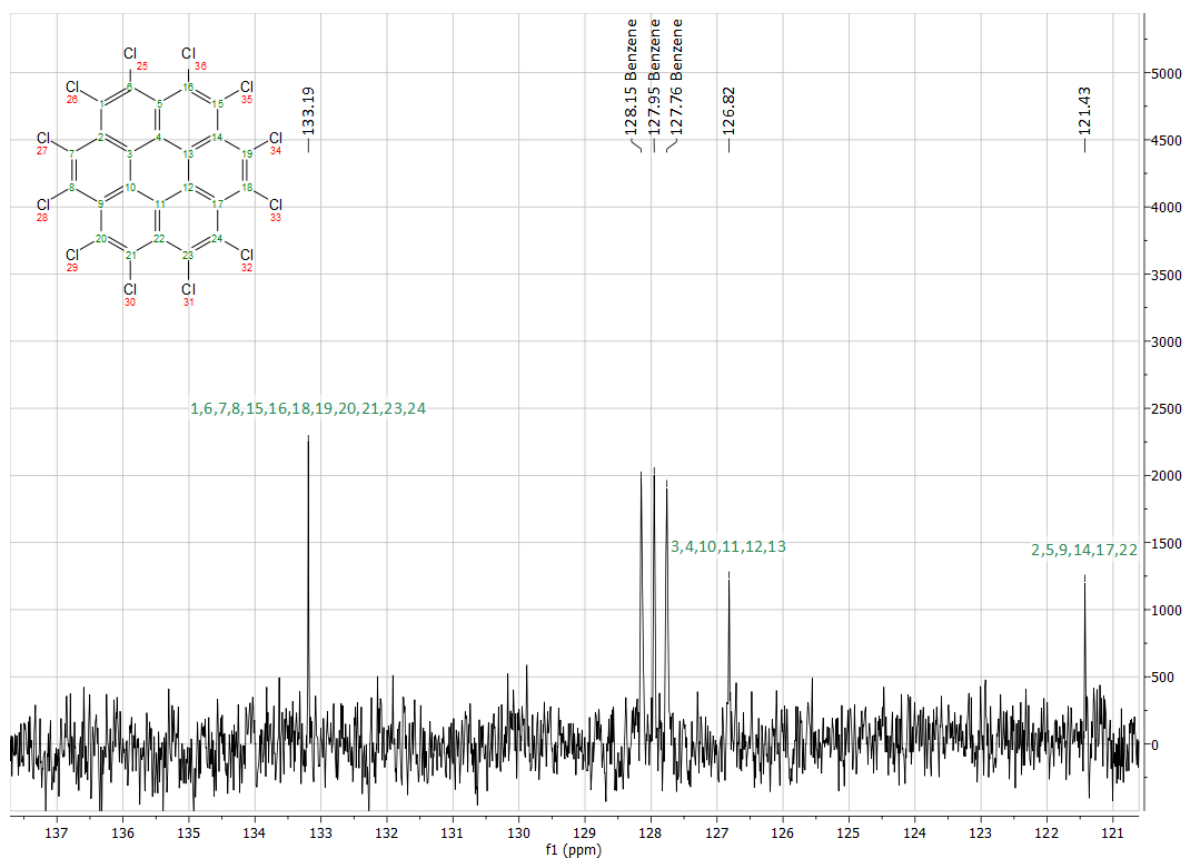


Figure 17. ^{13}C NMR for perchlorocoronene.

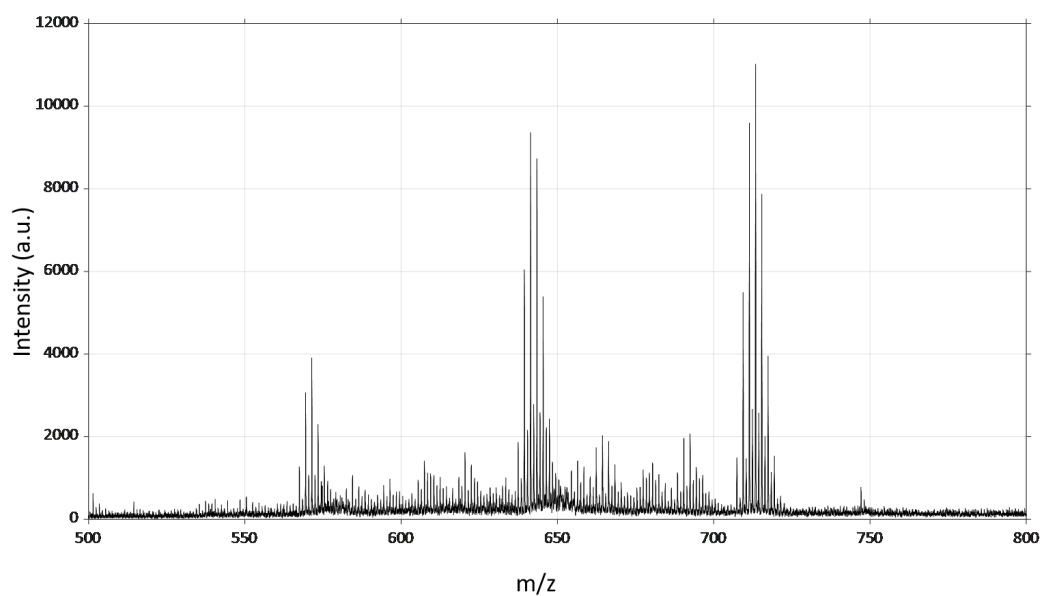


Figure 18. MALDI-ToF MS for perchlorocoronene.

6.2 H-HATN

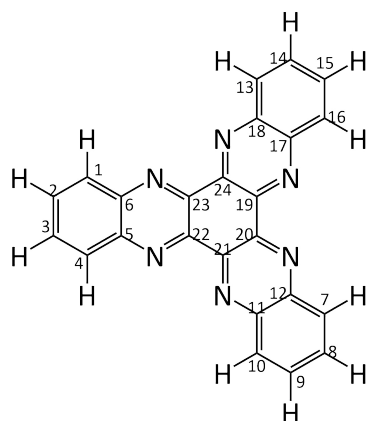


Figure 19. 5,6,11,12,17,18- hexaazatrinaphthylene.

H-HATN was prepared according to literature.⁹ 1,2-diaminobenzene (31.2 mg, 0.288 mmol) and hexaketocyclohexane octahydrate (30 mg, 0.096 mmol) were refluxed in 1:1 glacial acetic acid/ethanol (3 mL) for 24 hrs at 140 °C. After reflux, the blue reaction mixture was filtered under reduced pressure while hot and washed with hot glacial acetic acid (118 °C, 50 mL) until the filtrate was colourless. The resulting green solid was refluxed in nitric acid (30%, 5 mL) at 90 °C for 3 hrs. Upon mixing, the solid and nitric acid solvent turned bright yellow. After reflux, 5,6,11,12,17,18- hexaazatrinaphthylene was recovered as a yellow solid by filtering under reduced pressure and washed with deionised water (10 mL), then dried under vacuum (12.1 mg, 0.0315 mmol, 33%). ¹H NMR (CDCl₃, 400 MHz) δ 8.71 (6H, dd, J 6.53, J 3.51, H-1), 8.06 (6H, dd, J 6.59, J 3.45, H-2). ¹³C NMR (CDCl₃, 101 MHz) δ 143.74 (s, 5), 143.71 (s, 19), 132.44 (s, 1), 130.82 (s, 2). m/z 384.1 (C₂₄H₁₂N₆⁻, 100%), 279.9 (C₁₈H₈N₄⁻, 11.6%). IR (ATR)/cm⁻¹ ν_{max} : 3060 (C–H).

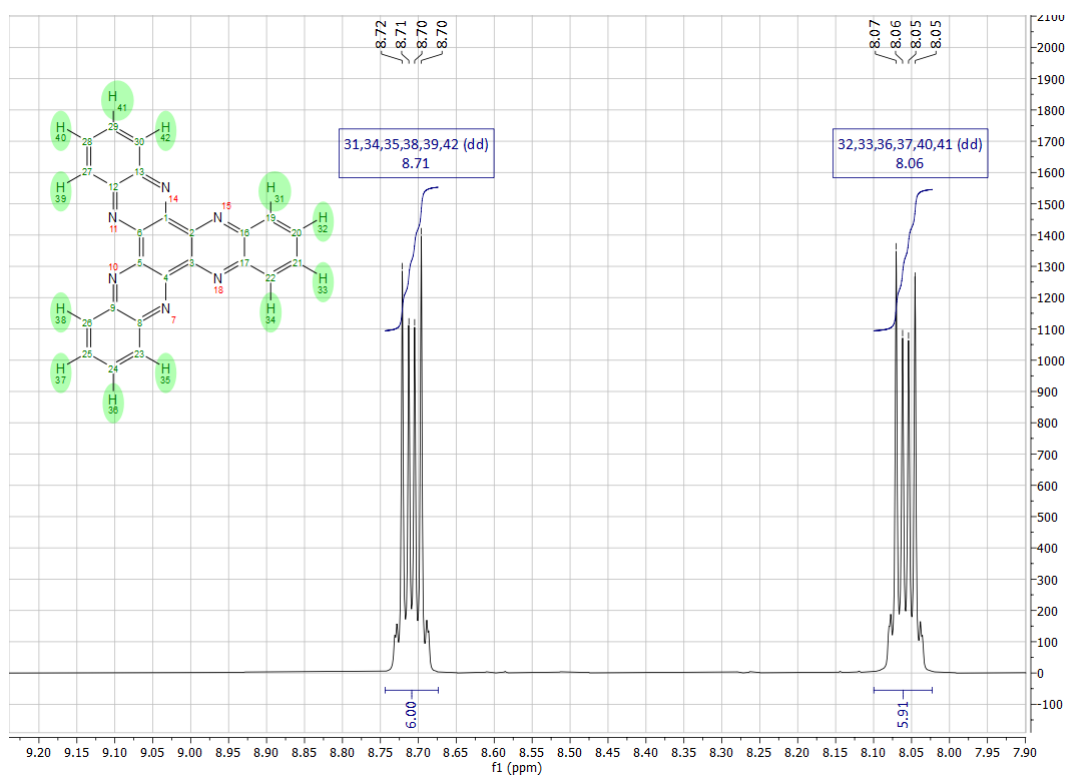


Figure 20. ^1H NMR for 5,6,11,12,17,18- hexaazatrinaphthylene.

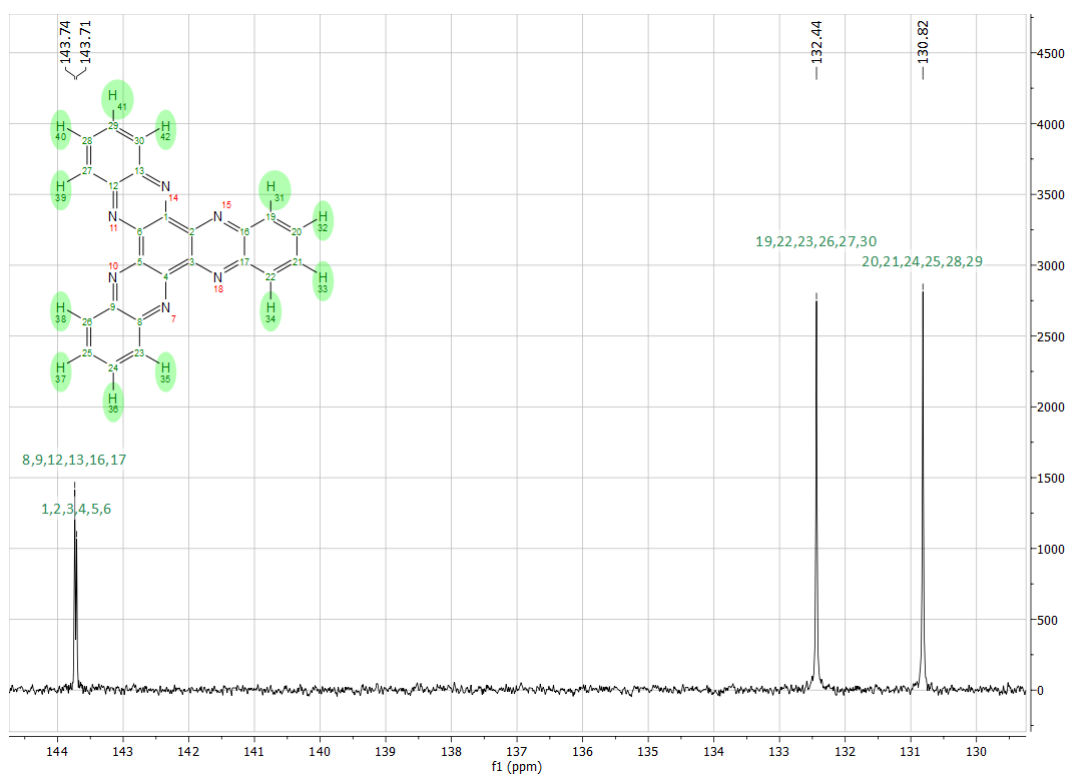


Figure 21. Proton-decoupled ^{13}C NMR for 5,6,11,12,17,18- hexaazatrinaphthylene.

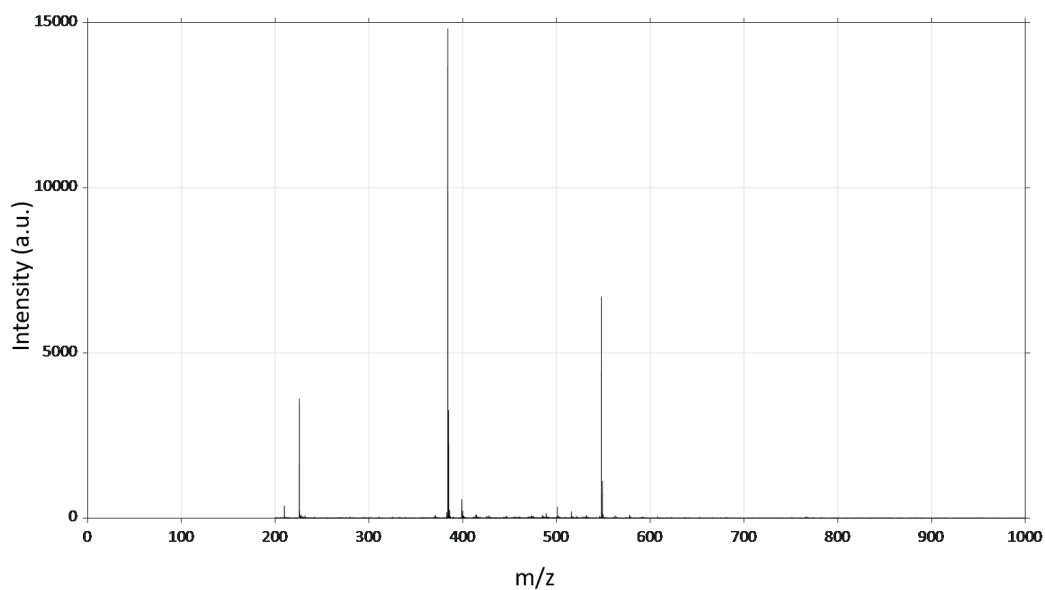


Figure 22. MALDI-ToF MS for 5,6,11,12,17,18- hexaazatrinaphthylene.

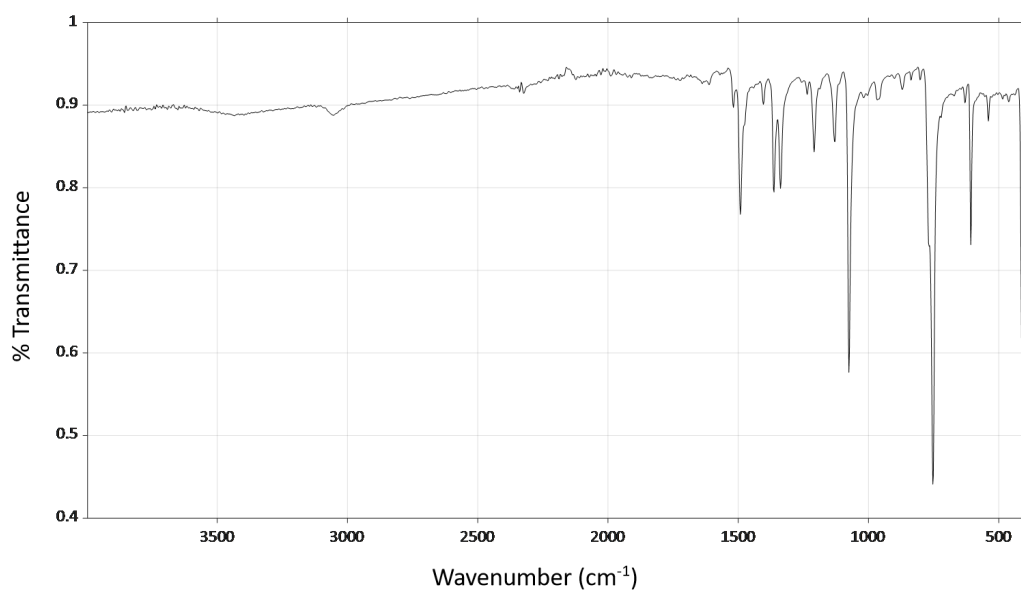


Figure 23. IR for 5,6,11,12,17,18- hexaazatrinaphthylene.

6.3 Cl₆-HATN

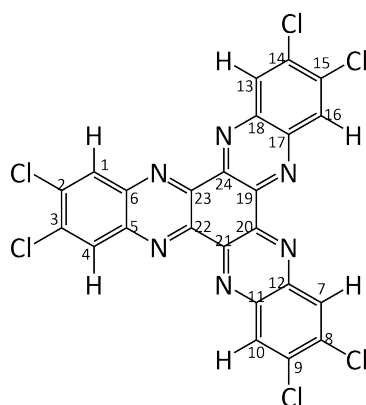


Figure 24. 2,3,8,9,14,15- hexachloro- 5,6,11,12,17,18- hexaazatrinaphthylene.

Cl₆-HATN was prepared according to literature.⁹ 4,5-dichloro-1,2-diaminobenzene (95.4 mg, 0.54 mmol) and hexaketocyclohexane octahydrate (31.4 mg, 0.101 mmol) were refluxed in 1:1 glacial acetic acid/ethanol (3 mL) for 24 hrs at 140 °C. Upon mixing, a dark red suspension formed. After reflux, the resulting dark green reaction mixture was filtered under reduced pressure while hot and washed with hot glacial acetic acid (100 °C, 20 mL) to give a dark green solid and pale yellow filtrate. The solid was refluxed in nitric acid (30%, 8 mL) at 90 °C for 3 hrs, then filtered under reduced pressure and washed with deionised water (10 mL) to yield a colourless filtrate and bright green solid (46.8 mg, 0.0792 mmol, 78 %). The green solid was then refluxed in glacial acetic acid (120 °C) for 1 hr, then filtered under reduced pressure while hot, washed with hot glacial acetic acid, then dried under reduced pressure to give 2,3,8,9,14,15-hexachloro- 5,6,11,12,17,18- hexaazatrinaphthylene as a bright yellow solid (37.5 mg, 0.0636 mmol, 22 %) ¹H NMR (CDCl₃, 400 MHz) δ 8.81 (6H, s, H-1). ¹³C NMR (CDCl₃, 101 MHz) δ 143.93 (s, 5), 142.36 (s, 19), 138.29 (s, 2), 131.00 (s, 1). m/z 589.1 (C₂₄H₆N₆Cl₆⁻, 100%). IR (ATR)/cm⁻¹ ν_{max} : 3090 (C–H).

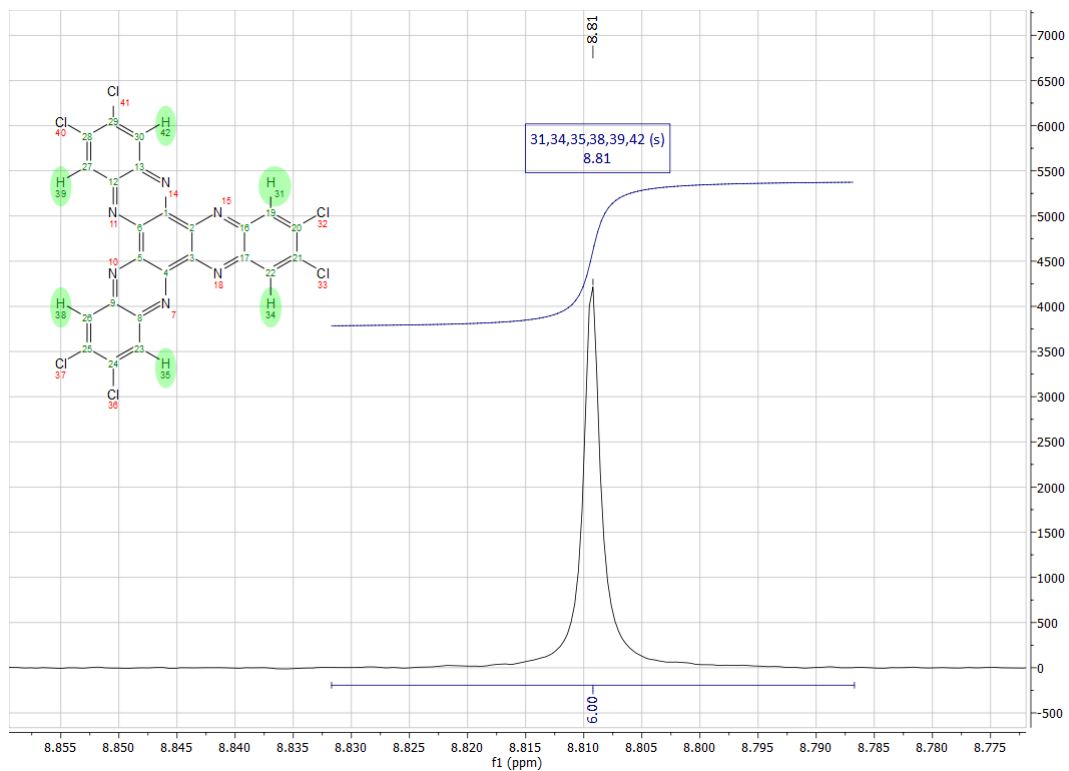


Figure 25. ^1H NMR for 2,3,8,9,14,15- hexachloro- 5,6,11,12,17,18- hexaazatrindaphthylene.

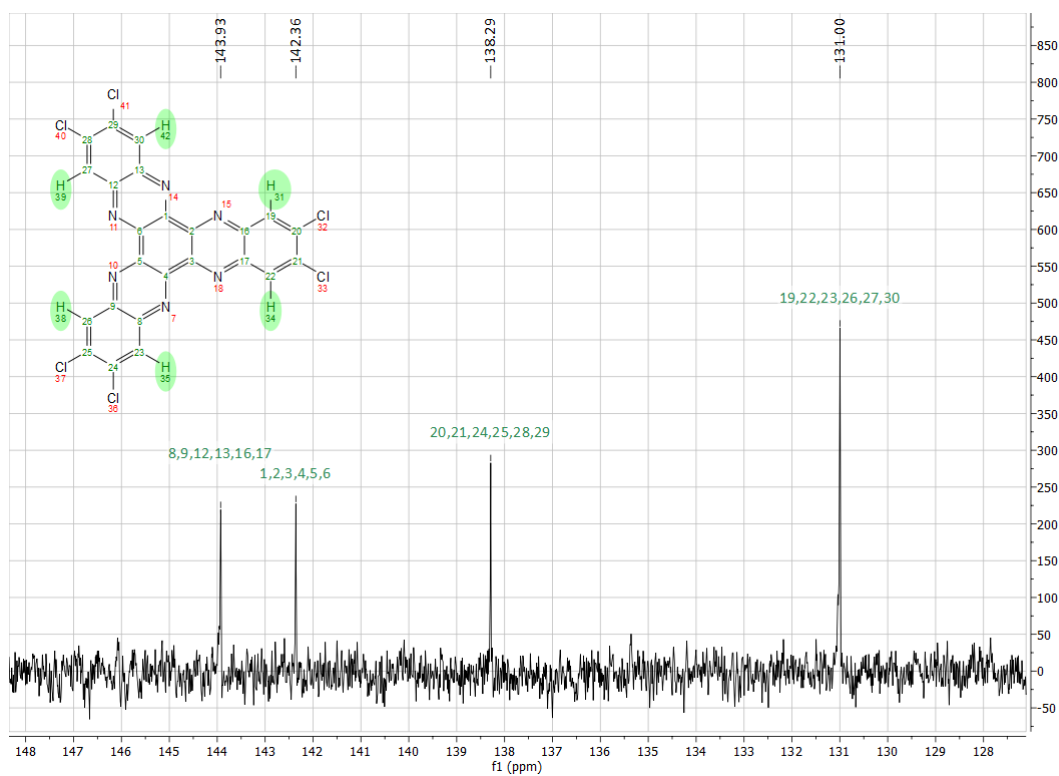


Figure 26. Proton-decoupled ^{13}C NMR for 2,3,8,9,14,15- hexachloro- 5,6,11,12,17,18- hexaazatrindaphthylene.

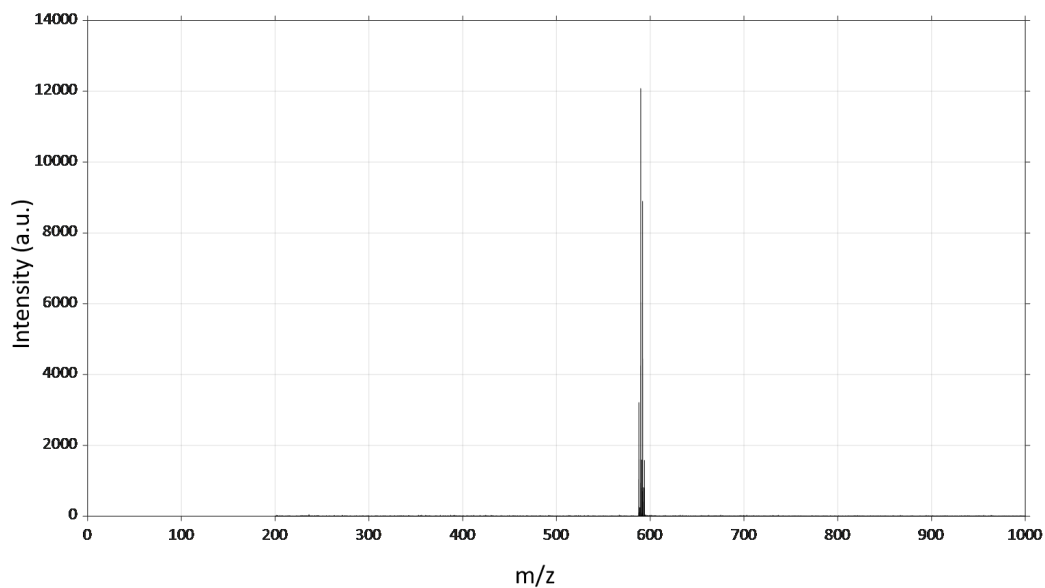


Figure 27. MALDI-ToF MS for 2,3,8,9,14,15- hexachloro- 5,6,11,12,17,18- hexaazatrinaphthylene.

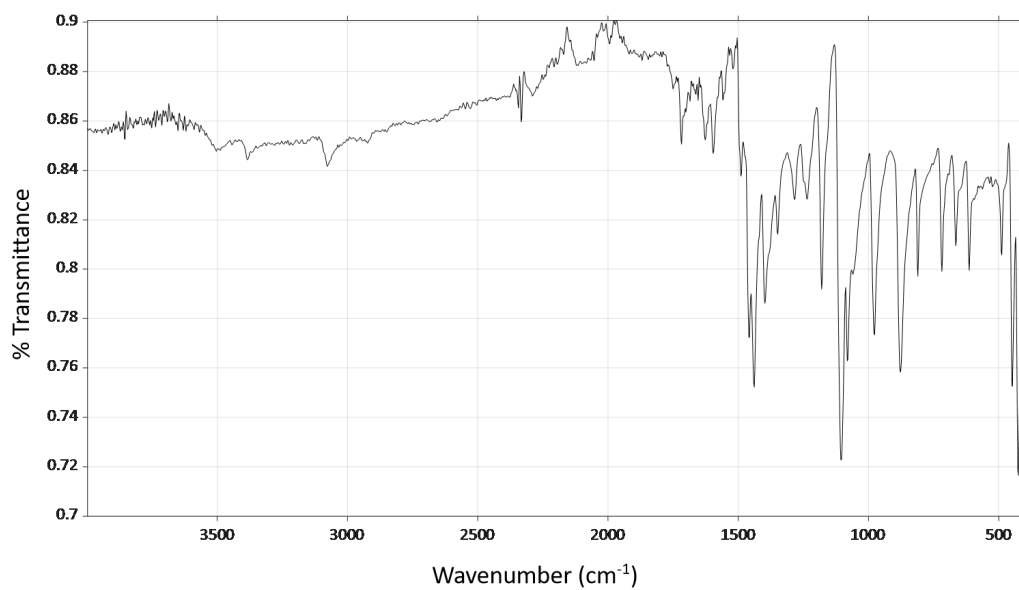


Figure 28. IR for 2,3,8,9,14,15- hexachloro- 5,6,11,12,17,18- hexaazatrinaphthylene.

6.4 F₆-HATN

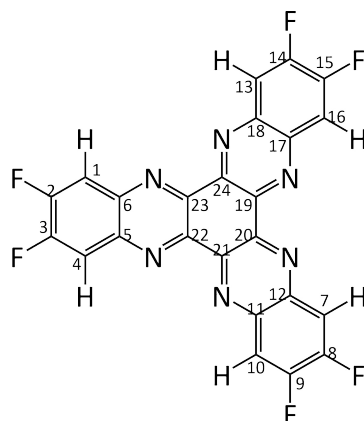


Figure 29. 2,3,8,9,14,15- hexafluoro- 5,6,11,12,17,18- hexaazatrinaphthylene.

F₆-HATN was prepared according to literature.⁹ 4,5-difluoro-1,2-diaminobenzene (43.8 mg, 0.304 mmol) and hexaketocyclohexane octahydrate (30 mg, 0.096 mmol) were refluxed in degassed glacial acetic acid (3 mL) for 16 hrs at 118 °C. After reflux, the dark purple reaction mixture was cooled to room temperature and filtered under reduced pressure. Washing with room temperature glacial acetic acid and drying under reduced pressure gave 2,3,8,9,14,15- hexafluoro- 5,6,11,12,17,18- hexaazatrinaphthylene as a grey-green solid (28.1 mg, 0.616 mmol, 64 %). ¹H NMR (CDCl₃, 400 MHz) δ 8.43 (6H, t, J 9.10, H-1). ¹⁹F NMR (CDCl₃, 400 MHz) δ -122.95 (6F, t, J 9.10, F-2). ¹⁹F(H) NMR (CDCl₃, 400 MHz) δ -122.96 (6F, s, F-2). ¹³C NMR (CDCl₃, 101 MHz) δ 154.70 (dd, J 264.67, J 18.35, 2), 143.20 (s, 5), 141.61 (t, J 6.34, 19), 115.95 (dd, J 13.08, J 6.90, 1). m/z 492.1 (C₂₄H₆N₆F₆⁻, 100%). IR (ATR)/cm⁻¹ ν_{max}: 3041 (C–H).

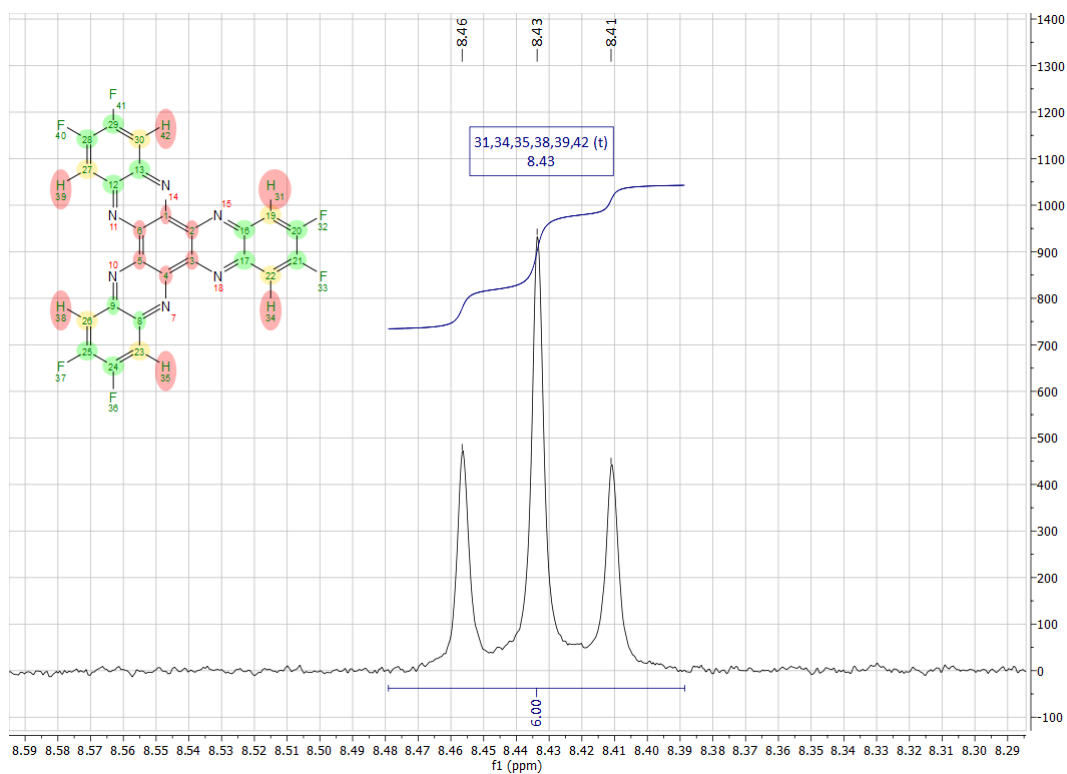


Figure 30. ^1H NMR for 2,3,8,9,14,15- hexafluoro- 5,6,11,12,17,18- hexaazatrinaphthylene.

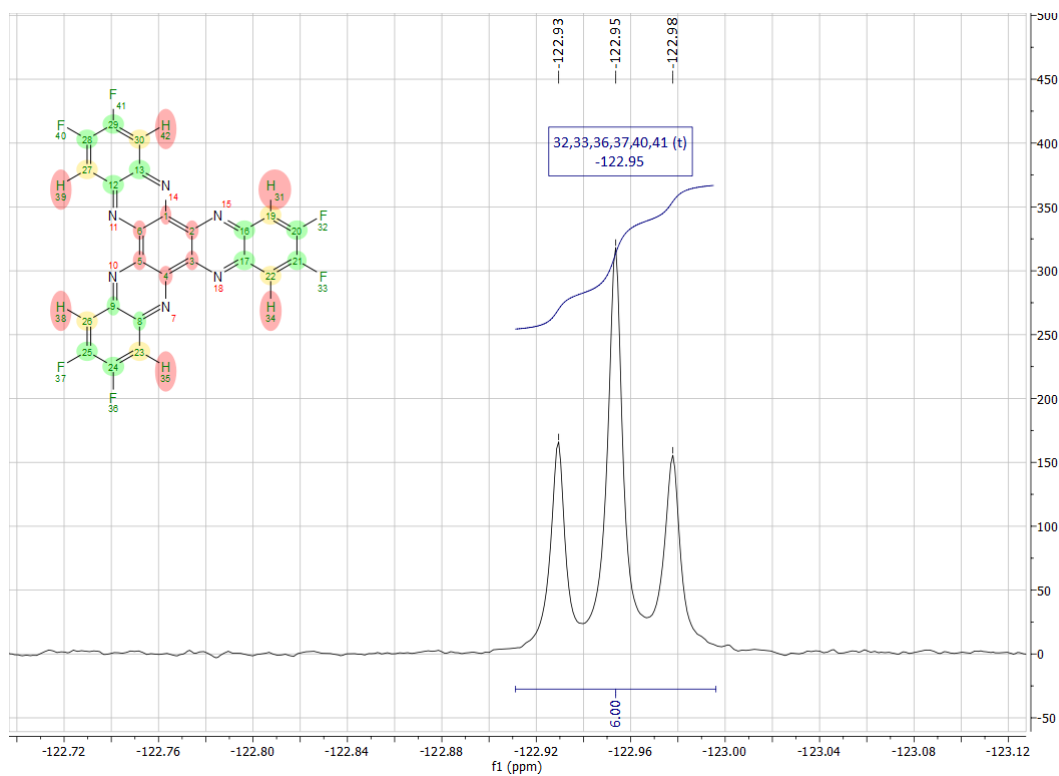


Figure 31. ^{19}F NMR for 2,3,8,9,14,15- hexafluoro- 5,6,11,12,17,18- hexaazatrinaphthylene.

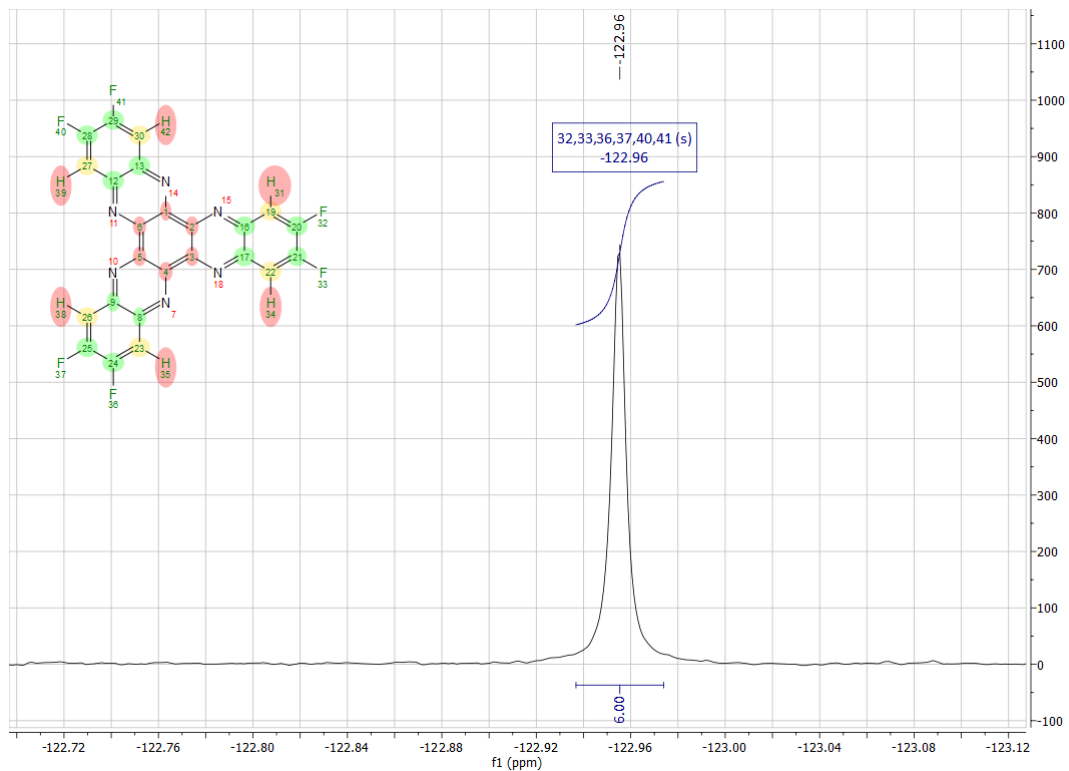


Figure 32. Proton-decoupled ^{19}F NMR for 2,3,8,9,14,15- hexafluoro- 5,6,11,12,17,18- hexaazatrinaphthylene.

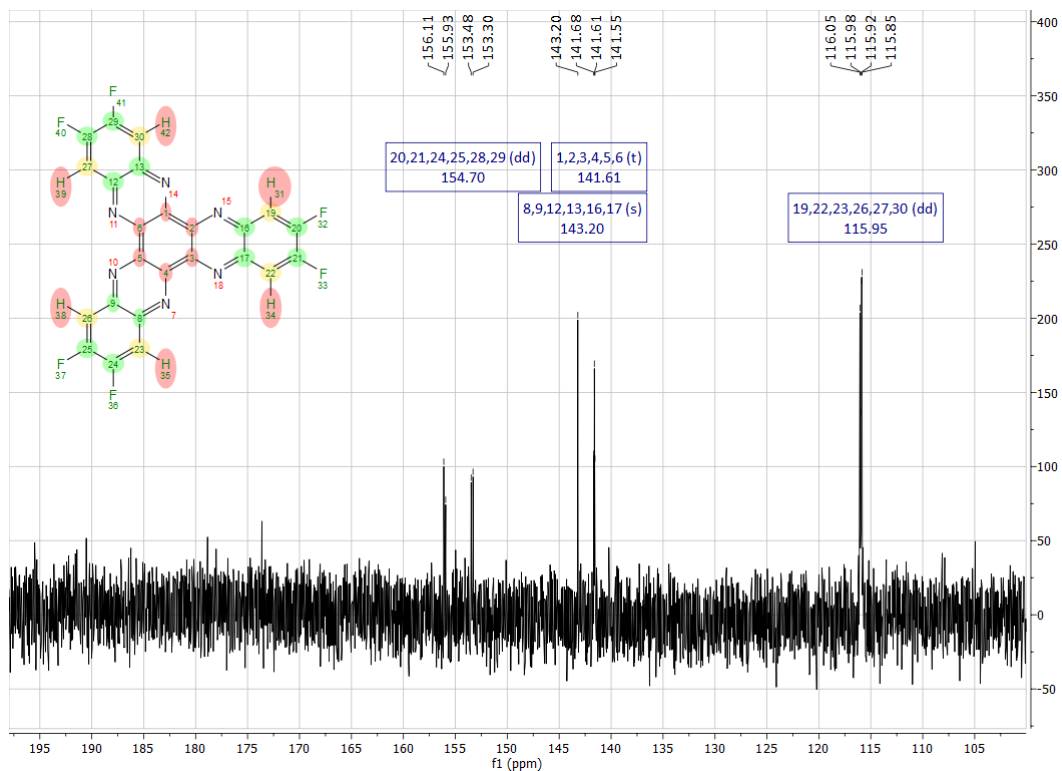


Figure 33. Proton-decoupled ^{13}C NMR for 2,3,8,9,14,15- hexafluoro- 5,6,11,12,17,18- hexaazatrinaphthylene.

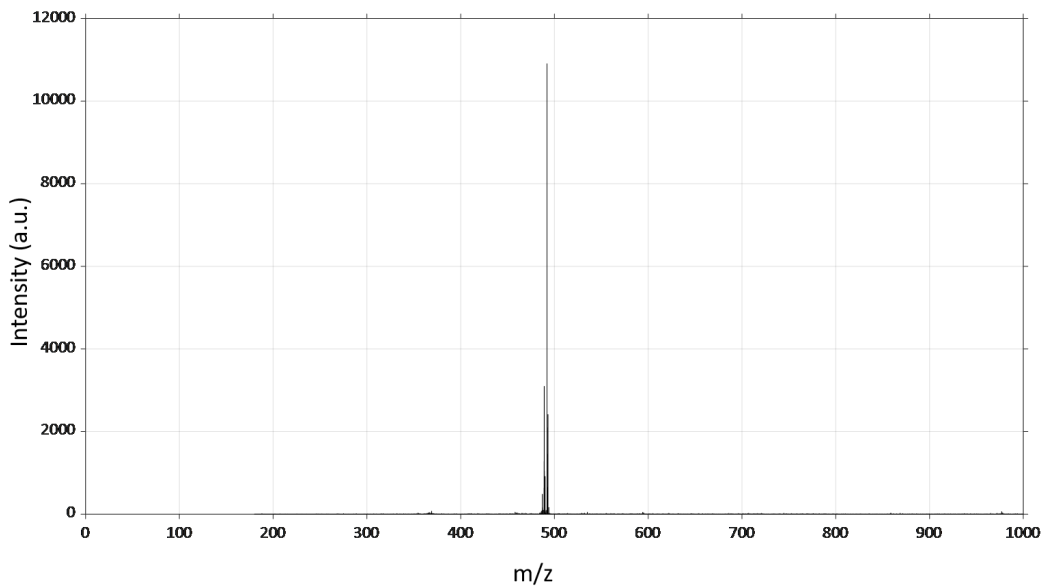


Figure 34. MALDI-ToF MS for 2,3,8,9,14,15- hexafluoro- 5,6,11,12,17,18- hexaazatrinaphthylene.

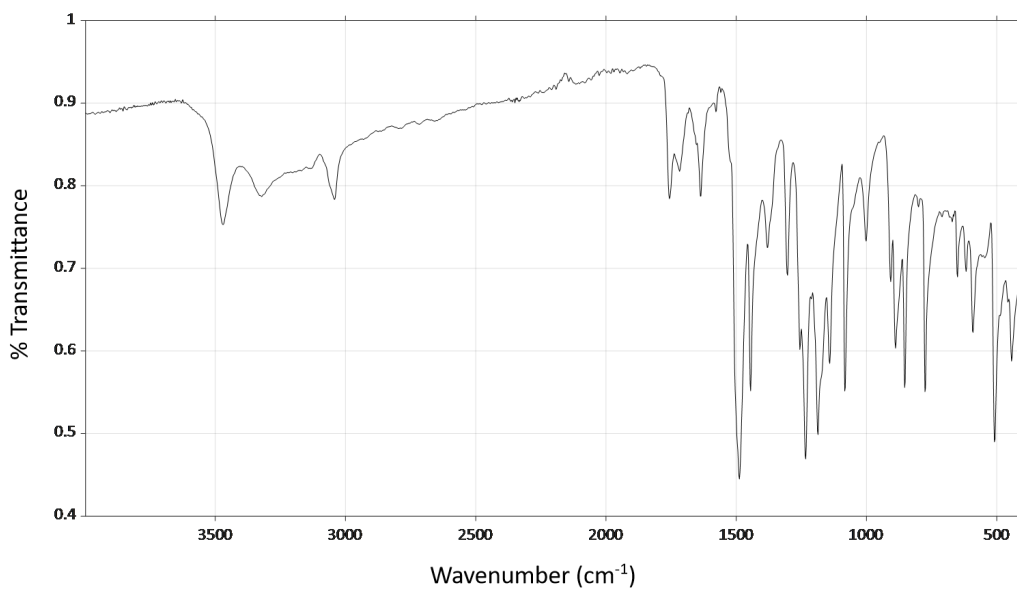


Figure 35. IR for 2,3,8,9,14,15- hexafluoro- 5,6,11,12,17,18- hexaazatrinaphthylene.

7 SCXRD refinement and data

7.1 Refinement details for 5,6,11,12,17,18- hexaazatrinaphthylene

The very fine needle-like crystals grown by sublimation diffracted weakly with a low-resolution diffraction limit, despite the use of synchrotron radiation. Restraints were applied to the geometry and anisotropic displacement parameters of the structure to aid refinement and support the consequently low data to parameter ratio of 5.36. The geometries of the two three-fold symmetric residues were restrained to have similar and symmetric geometries (SAME). Rigid bond and similarity restraints (RIGU, SIMU) were applied to the anisotropic displacement parameters of all atoms in the structure. All hydrogen atoms were geometrically placed and refined using a riding model.

7.2 Refinement details for 2,3,8,9,14,15- hexafluoro- 5,6,11,12,17,18- hexaazatrinaphthylene

The very thin lath-like crystals diffracted weakly despite the use of synchrotron radiation; the data used in the refinement was truncated to a resolution of 0.95 Å. All hydrogen atoms were observed in the electron density map. The aryl hydrogen atoms were geometrically placed before being refined with a riding model. The water hydrogen atoms are refined with their 1,2 and 1,3 distances restrained to have suitable geometries. The isotropic displacement parameters of all hydrogen atoms are fixed at $1.2 \times U_{eq}$ (aryl) and $1.5 \times U_{eq}$ (water) of their parent atoms. One of the hydrogen atoms of water O2W is disordered over two sites which are fixed at half occupancy each. The two disorder sites are parted such that the hydrogen atoms are in separate parts to their symmetry equivalents on adjacent water residues. One of the hydrogen atoms in O1W donates a hydrogen bond to an adjacent symmetry equivalent O1W residue. The hydrogen atom is modelled at half-occupancy and parted to be in a different disorder component to its symmetry equivalent. The remaining half-occupancy hydrogen site at O1W will likely donate a hydrogen bond to one of the other two proximate symmetry

equivalent O1W residues. This other hydrogen position is not apparent in the electron density map and is not included in the model, however, it is included in the unit cell contents all derived parameters.

7.3 SCXRD data for 5,6,11,12,17,18- hexaazatrinaphthylene and 2,3,8,9,14,15- hexafluoro- 5,6,11,12,17,18- hexaazatrinaphthylene.

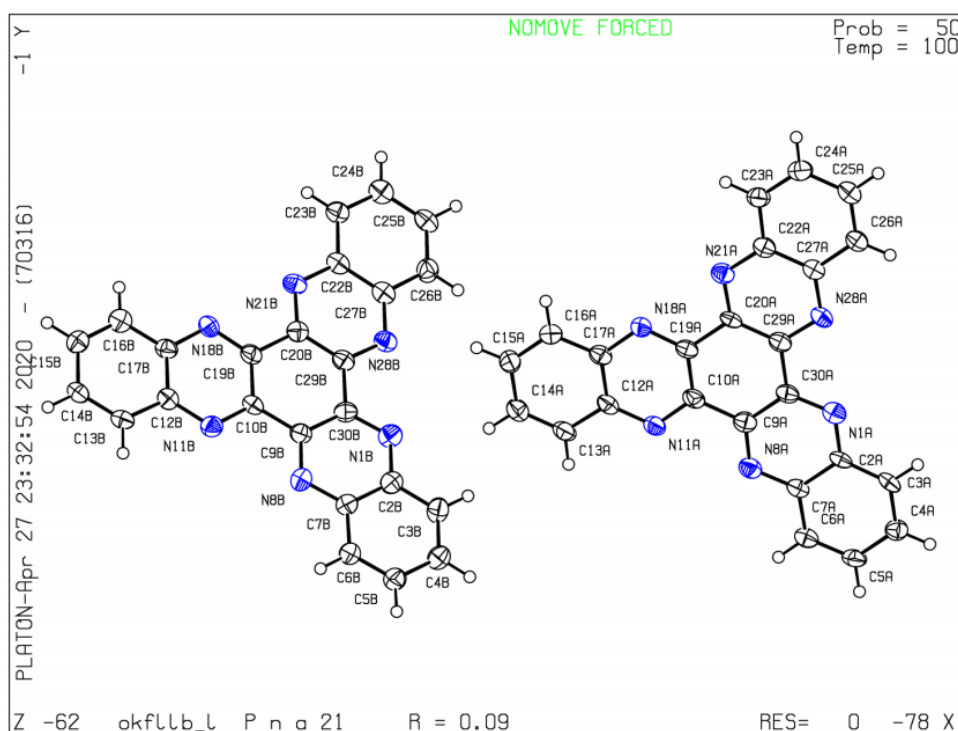


Figure 36. Ellipsoid plot of the unit cell of 5,6,11,12,17,18- hexaazatrinaphthylene.

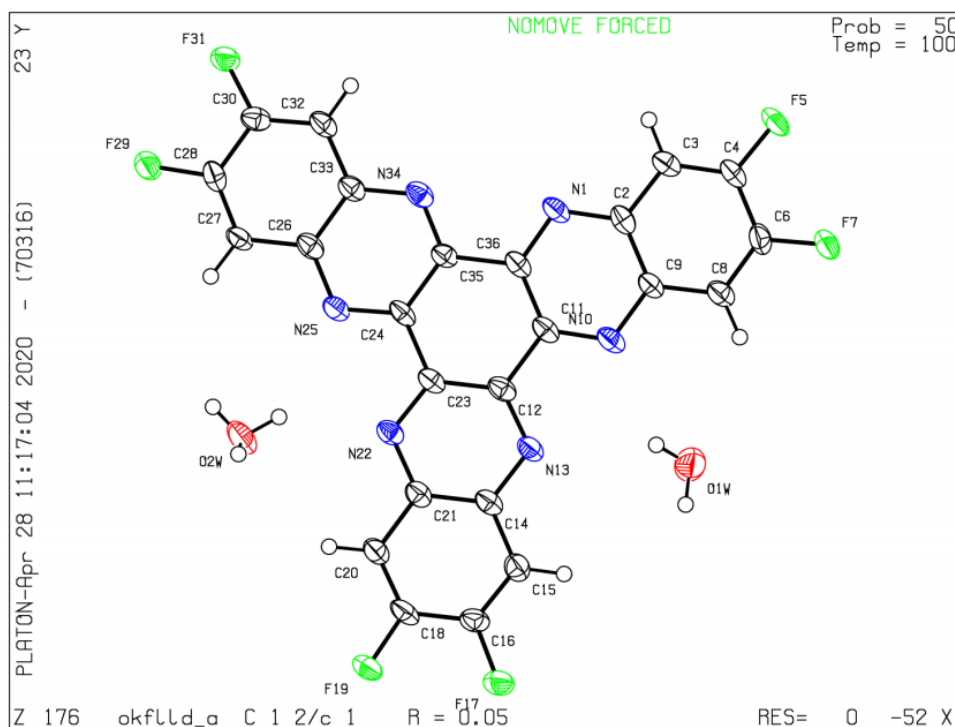


Figure 37. Ellipsoid plot of the unit cell of 5,6,11,12,17,18- hexaazatrinaphthylene.

Crystal data and structure refinement for 5,6,11,12,17,18- hexaazatrinaphthylene and 2,3,8,9,14,15- hexafluoro- 5,6,11,12,17,18- hexaazatrinaphthylene.

Add the CCDC deposition numbers to these tables when they are obtained ahead of submission of the manuscript.

Empirical formula	$C_{24}H_{12}N_6$	$C_{24}H_{10}F_6N_6O_2$
Formula weight	384.40	528.38
Temperature/K	100(2)	100(2)
Crystal system	orthorhombic	monoclinic
Space group	$Pna2_1$	$C2/c$
$a/\text{\AA}$	21.7922(18)	34.4280(6)
$b/\text{\AA}$	3.8884(3)	4.48900(10)
$c/\text{\AA}$	39.449(3)	29.9864(4)
$\alpha/^\circ$	90.0	90
$\beta/^\circ$	90.0	120.1050(10)
$\gamma/^\circ$	90.0	90
Volume/ \AA^3	3342.8(3)	4009.18(13)

Z	8	8
$\rho_{\text{calc}}/\text{cm}^3$	1.528	1.751
μ/mm^{-1}	0.090	0.144
F(000)	1584.0	2128.0
Crystal size/ mm^3	$0.15 \times 0.005 \times 0.002$	$0.2 \times 0.005 \times 0.005$
Synchrotron radiation	$\lambda=0.6889$	$\lambda=0.6889$
2θ range for data collection/ $^\circ$	2.002 to 47.798	4.604 to 42.51
Index ranges	$-25 \leq h \leq 25, -4 \leq k \leq 4,$ $-46 \leq l \leq 46$	$-36 \leq h \leq 34, -4 \leq k \leq 4,$ $-31 \leq l \leq 31$
Reflections collected	30591	6742
Independent reflections	5690 [$R_{\text{int}} = 0.1654, R_{\text{sigma}} = 0.0973$]	2401 [$R_{\text{int}} = 0.0483, R_{\text{sigma}} = 0.0641$]
Data/restraints/parameters	5690/1891/542	2401/8/358
Goodness-of-fit on F^2	1.040	1.044
Final R indexes [$I \geq 2\sigma(I)$]	$R_1 = 0.0908, wR_2 = 0.2209$	$R_1 = 0.0522, wR_2 = 0.1451$
Final R indexes [all data]	$R_1 = 0.1197, wR_2 = 0.2379$	$R_1 = 0.0676, wR_2 = 0.1541$
Largest diff. peak/hole/ $\text{e}\text{\AA}^{-3}$	0.42/−0.32	0.32/−0.29
Flack parameter	−0.7(10)	

References

1. J. Schindelin, I. Arganda-Carreras, E. Frise, V. Kaynig, M. Longair, T. Pietzsch, S. Preibisch, C. Rueden, S. Saalfeld, B. Schmid, J. Y. Tinevez, D. J. White, V. Hartenstein, K. Eliceiri, P. Tomancak and A. Cardona, *Nat. Methods*, 2012, **9**, 676–682.
2. J. Schindelin, C. T. Rueden and M. C. Hiner, *Mol. Reprod. Dev.*, 2015, **82**, 518–529.
3. C. A. Schneider, W. S. Rasband and K. W. Eliceiri, *Nat. Methods*, 2012, **9**, 671–675.
4. M. Klinger and A. Jäger, *J. Appl. Crystallogr.*, 2015, **48**.
5. M. Klinger, *CrysTBox - Crystallographic Toolbox*, Institute of Physics of the Czech Academy of Sciences, 2015.
6. M. Klinger, M. Němec, L. Plívka, V. Gärtnerová and A. Jäger, *Ultramicroscopy*, 2015, **150**, 88–95.
7. T. Baird, J. H. Gall, D. D. MacNicol, P. R. Mallinson and C. R. Michie, *J. Chem. Soc., Chem. Commun.*, 1988, 1471–1473.
8. J. K. Fawcett and J. Trotter, *Proc. R. Soc. Lond. A*, 1966, **289**, 366–376.
9. S. Barlow, Q. Zhang, B. R. Kaafarani, C. Risko, F. Amy, C. K. Chan, B. Domercq, Z. A. Starikova, M. Y. Antipin, T. V. Timofeeva, B. Kippelen, J.-L. Brédas, A. Kahn and S. R. Marder, *Chem. Eur. J.*, 2007, **13**, 3537–3547.
10. M. Ballester and C. Molinet, *C. Chem. Ind. (London)*, 1954, 1290.
11. M. Koshino, H. Kurata and S. Isoda, *Ultramicroscopy*, 2010, **110**, 1465–1474.